

Pre-main sequence stars in the Cepheus flare region

Mária Kun

Konkoly Observatory, H-1121 Budapest, Konkoly Thege út 15–17, Hungary

kun@konkoly.hu

Zoltán Balog^{*†}

Steward Observatory 933 N. Cherry Av. Tucson, AZ, USA

Scott J. Kenyon

Harvard–Smithsonian CfA, 60 Garden St. Cambridge, MA, USA

Eric E. Mamajek

Department of Physics & Astronomy, University of Rochester, Rochester, NY, 14627-0171 USA

Robert A. Gutermuth

Harvard–Smithsonian CfA, 60 Garden St. Cambridge, MA, USA

ABSTRACT

We present results of optical spectroscopic and BVR_CI_C photometric observations of 77 pre-main sequence (PMS) stars in the Cepheus flare region. A total of 64 of these are newly confirmed PMS stars, originally selected from various published candidate lists. We estimate effective temperatures and luminosities for the PMS stars, and comparing the results with pre-main sequence evolutionary models we estimate stellar masses of 0.2–2.4 M_\odot and stellar ages of 0.1–15 Myr. Among the PMS stars, we identify 15 visual binaries with separations of 2–10 arcsec. From archival IRAS, 2MASS, and Spitzer data, we construct their spectral energy distributions and classify 5% of the stars as Class I, 10% as Flat SED, 60% as Class II, and 3% as Class III young stellar objects (YSOs). We identify 12 CTTS and 2 WTTS as members of NGC 7023, with mean age of 1.6 Myr. The 13 PMS stars associated with L 1228 belong to three small aggregates: RNO 129, L 1228 A, and L 1228 S. The age distribution of the 17 PMS stars associated with L 1251 suggests that star formation has propagated with the expansion of the Cepheus flare shell. We detect sparse aggregates of ~ 6 –7 Myr-old PMS stars around

^{*}On leave from Dept. of Optics and Quantum Electronics, University of Szeged, Dóm tér 9, Szeged, Hungary

[†]Present address: Max-Planck-Institut für Astronomie, Königstuhl 17, D-69117 Heidelberg, Germany

the dark clouds L 1177 and L 1219, at a distance of ~ 400 pc. Three T Tauri stars appear to be associated with the Herbig Ae star SV Cep at a distance of 600 pc. Our results confirm that the molecular complex in the Cepheus flare region contains clouds of various distances and star forming histories.

Subject headings: stars: formation– stars: pre-main sequence– ISM: clouds –ISM: individual (Cepheus flare)

1. Introduction

Star forming regions in our Galactic environment offer a unique opportunity for understanding the birth of planetary systems. There is growing evidence that not only the stellar content and structure of young stellar groups, but also the evolution of protostellar envelopes and accretion disks depend on the star forming environment (e.g. Hester & Desch 2005; Dullemond et al. 2006). Cross-comparing various star forming environments is important for understanding the origins and early evolution of stars and planets. In this paper we present our results of spectroscopic and photometric studies of a population of pre-main sequence stars associated with the molecular clouds of the Cepheus flare, located at 200–400 pc from the Sun.

A detailed review on the ISM and young stellar populations in the Cepheus flare region can be found in Kun, Kiss, & Balog (2008). Here we briefly review the highlights that are relevant for this study. The Cepheus flare (Hubble 1934) molecular cloud complex consists of a large amount of dense ISM between $100^\circ \leq l \leq 120^\circ$ and above $b \geq 10^\circ$ (Lynds 1962; Taylor, Dickman & Scoville 1987; Clemens & Barvainis 1988; Dobashi et al. 2005). Though the CO maps of the region presented by Lebrun (1986) and Grenier et al. (1989) indicate a coherent cloud complex, there is evidence for multiple cloud layers over the Cepheus flare region. For instance, stars illuminating reflection nebulae or displaying $100 \mu\text{m}$ excess due to their dusty environment, can be found at various distances (e.g. Racine 1968; Kun, Vinkó & Szabados 2000), suggesting the presence of more than one dust layer between about 200 and 800 pc. Wolf diagrams of the region indicate extinction layers at 200, 300, and about 450 pc (Kun 1998). Radial velocity measurements of the interstellar matter suggest the presence of several gas layers (e.g. Heiles 1967; Yonekura et al. 1997). Olano et al. (2006) modeled the space distribution and kinematics of the interstellar neutral and molecular gas by an expanding shell, centered on $(l, b) \approx (120^\circ, +17^\circ)$, at a distance of about 300 pc. The presence of the *Cepheus flare Shell* (CFS), an old supernova remnant, readily explains the divergent cloud distances and the wide range of radial velocities. The giant radio continuum feature *Loop III* (Berkhuijsen 1973; Spoelstra 1973), conspicuous in the *WMAP* K-band polarization map (Page et al. 2007), is nearly concentric with the molecular shell. Several giant far-infrared loops, possibly old supernova shells, have been identified in the IRAS images of the Cepheus flare region (Kiss et al. 2004).

Signposts of low-mass star formation in the Cepheus flare region have been detected in the

molecular clouds L 1082 (B 150, GF 9), L 1148/L 1158, L 1172/L 1174 (associated with the young cluster NGC 7023), L 1228, L 1177 (CB 230), L 1219 (B 175), L 1221, L 1251, and L 1261 (CB 244) (see review of Kun et al. 2008). Recently, Kirk et al. (2009) presented a list of 133 young stellar objects and candidates, based on Spitzer observations of L 1148/L 1158, L 1172/L 1174, L 1228, L 1221, and L 1251. Independent distance estimations of individual clouds suggest various distances between 150 and 500 pc, but are clustered around 300 pc. The young open cluster NGC 7129, associated with the dark cloud L 1181, is projected on the Cepheus flare region at $(l,b)=(105.4,+9.9)$, but is more distant than the bulk of clouds (800–1250 pc, see Kun et al. (2008)). The central region of the complex is lacking signatures of active star formation. The physical connection between the star-forming clouds remains rather uncertain.

Scarce information is available on the pre-main-sequence (PMS) stellar population of the region. Herbig & Bell (1988) list only 14 young objects in the Cepheus flare region: RNO 124 and PV Cep (associated with the cloud complex L 1148/L 1158), HD 200775, EH Cep, FU Cep, FV Cep (members of NGC 7023), LkH α 234, BD +65 $^{\circ}$ 1637, V350 Cep, [SVS76] NGC 7129 6 (members of NGC 7129), AS 507 (associated with L 1261), and the apparently isolated Herbig Ae/Be stars BH Cep, BO Cep, and SV Cep. Six further stars in NGC 7129 (MEG 1–MEG 3, [HL85] 14: Miranda et al. 1993; GGD 33a: Miranda et al. 1994, and V391 Cep: Semkov 1993) show T Tauri-like emission spectra, but no spectral types have been given for them in the literature. Tachihara et al. (2005) identified 16 weak-line T Tauri stars in the region, by spectroscopic and photometric follow-up studies of X-ray emitting stars found in the ROSAT database. These stars are not obviously associated with any dark cloud. Understanding star formation in each dark cloud and relating star formation rates across the dark clouds requires a comprehensive deep survey.

Here, we use optical and infrared observations to develop a better picture of star formation in this region. To constrain the nature of the candidate young stars, we combine new optical spectroscopy and BVRI photometry with archival infrared data from IRAS, 2MASS, and Spitzer. We describe our observations and data reduction in Sect. 2. We use these data to estimate ages, luminosities, masses, and disk properties of individual young stars and to analyze the distributions of these physical parameters among each cloud. Section 3 contains the main results, namely the HR diagrams and spectral energy distributions of the target stars. We discuss the implications of our results for the star formation history of the region in Sect. 4.

2. Observations and data reduction

2.1. Target selection

Several lists of potential PMS stars, such as H α emission stars detected by objective prism surveys, irregular variables, far- and mid-infrared sources can be found in the literature. The targets of our studies are the stars brighter than about $V = 16$ mag from the lists as follows: irregular variables associated with NGC 7023 (Rosino & Romano 1962) and NGC 7129 (Semkov 2003), H α

emission stars associated with L 1228 (Ogura & Sato 1990), L 1251 (Kun & Prusti 1993), NGC 7129 (Magakian et al. 2004), and distributed over the whole area of the Cepheus flare (Kun 1998), nebulous stars associated with L 1251 (Eiroa et al. 1994); IRAS point sources of T Tauri-like flux ratios, distributed over the whole region (Kun 1998), near-infrared sources associated with L 1251 (Rosvick & Davidge 1995), and Spitzer sources associated with L 1228 S (Padgett et al. 2004). In addition we found four new K_s band-excess stars in the 2MASS (Cutri et al. 2003) database, not coinciding with previously identified PMS star candidates (2MASS 21223461+6921142, 21225427+6921345, 21544662+6708255, and 22283821+7119023). Only one of them (2MASS 21225427+6921345) was sufficiently bright in the optical wavelengths for our spectroscopic observations. In all, we observed spectra of 170 stars, including 13 confirmed PMS stars of the region. Spectral types for some of these latter stars were presented by Cohen & Kuhi (1979) and Mora et al. (2001), however no previous studies have presented spectroscopy of the red part of the optical spectrum nor BVR_CI_C photometry for these stars.

The accuracy of the target coordinates given in the source papers and in the SIMBAD database is typically several arcseconds. Therefore we used the published finding charts of the objects with the DSS to refine the coordinates, and then used these improved coordinates to find the associated 2MASS source (usually with positional accuracy of $<0''.2$).

2.2. Spectroscopy

2.2.1. CAFOS spectra

Spectra of 155 stars were observed using the CAFOS instrument on the 2.2-m telescope of Calar Alto Observatory between 1999 August 7–11, 2004 August 10–15, 2005 September 11–14, and 2008 August 26–31. At some target positions two stars can be found within a few arcseconds. We obtained spectra of both stars provided both were sufficiently bright. During the observing run in 1999 we used the G–100 grism, covering the wavelength range 5000–7000 Å. Observations in 2004–2008 were performed through the R–100 grism, covering the wavelength interval 5800–9000 Å. The spectral resolution of CAFOS observation, using a 1.5-arcsec slit, was $\lambda/\Delta\lambda \approx 3500$ at $\lambda = 6600$ Å. We estimated the exposure time required for obtaining $S/N \approx 50$ at 6600 Å based on the available optical magnitudes of the target stars. The spectrum of a He–Ne–Rb lamp was regularly observed for wavelength calibration. We reduced and analysed the spectra using standard IRAF¹ routines.

The wavelength range of spectra taken with the R–100 grism was suitable for determining several flux ratios defined for spectral classification by Kirkpatrick, Henry & McCarthy (1991) (A ,

¹IRAF is distributed by the National Optical Astronomy Observatories, which are operated by the Association of Universities for the Research in Astronomy, Inc., under cooperative agreement with the National Science Foundation. <http://iraf.noao.edu/>

B , C , B/A , B/C), Martín & Kun (1996) (I_2 , I_3), and Preibisch et al. (2001) ($T1$, $T2$). We measured these spectral features on the spectra of our stars, and calibrated them against the spectral type and luminosity class by measuring them in a series of standard stars published by Le Borgne et al. (2003). Each flux ratio resulted in an estimate of spectral type, and we adopted as final spectral type the average of those inferred from the individual flux ratios. The accuracy of our spectral classification, estimated from the range of spectral types obtained from different flux ratios, is ± 1 subclass. We have not tried to correct the classification for the veiling. The above spectral indices can be used for classification of stars later than about K5. The brighter, and thus possibly earlier type, stars of the region were therefore observed with other instruments, covering shorter wavelengths. To classify K-type stars in the CAFOS+R-100 sample we used the Ca I lines at 6122 and 6161 Å. Spectral classification criteria for the spectra obtained with G-100 grism included the Mg I, Na I, and Ca I lines. Preliminary results of the classification of these stars were presented in Eredics & Kun (2003).

2.2.2. *FLWO spectra*

With the help of the FLWO staff (P. Berlind, M. Calkins) we acquired low-resolution optical spectra of 46 target stars with FAST, a high throughput slit spectrograph mounted on the Fred L. Whipple Observatory 1.5-m telescope on Mount Hopkins, Arizona (Fabricant et al. 1998). In addition to the candidate PMS stars, we observed the spectrum of VDB 141, a star illuminating a reflection nebula near L 1177, whose spectral type is not included in Racine’s (1968) list of reflection nebulae. We used a 300 g mm⁻¹ grating blazed at 4750 Å, a 3'' slit, and a thinned Loral 512 × 2688 CCD. These spectra cover 3800–7500 Å at a resolution of ~ 6 Å. We reduced and analysed the spectra with IRAF. After trimming the CCD frames at each end of the slit, we corrected for the bias level and flat-field for each frame, applied an illumination correction, and derived a full-wavelength solution from calibration lamps acquired immediately after each exposure. The wavelength solution for each frame has a probable error of ± 0.5 –1.0 Å. To construct final 1-D spectra, we extracted object and sky spectra using the optimal extraction algorithm within APEXTRACT. Most spectra have moderate signal-to-noise per pixel ($S/N \sim 30$). Using the method described by Balog & Kenyon (2002), we detected H α emission in the spectra of 22 stars. The spectral classification was performed by visually comparing the spectra of MK standard stars with our candidates following the procedure described by Jaschek & Jaschek (1987).

2.2.3. *The final list of PMS stars*

We accepted an object as a classical T Tauri star if it fulfilled the criterion established by Barrado y Navascués & Martín (2003), i.e. EW(H α) exceeded the saturation limit of the chromospheric activity, depending on the spectral type. The H α emission of such stars is thought to originate from the gas accreted by the star from the disk. Many of our target stars claimed to be

H α emission stars based on objective prism observations (Ogura & Sato 1990; Kun 1998) proved to be M-type dwarfs with $EW(H\alpha) < 10 \text{ \AA}$, evolved stars, or stars without H α emission. Part of these latter stars may be PMS objects with variable H α emission. Possibly such an object is K98c Em* 132, a K-type star whose H α absorption line is filled in by emission (see Fig. 1). We excluded these stars from the further study, unless the Li I λ 6708 line was conspicuous in their spectrum or some evidence of youth (strong X-ray emission, infrared excess) could be found in the literature. Strong Li I absorption in low resolution spectra alone is not sufficient criterion of the PMS nature, given that blending with several neighboring lines may result in a large apparent equivalent width. Therefore we regard the M-type stars whose $EW(H\alpha) < 10 \text{ \AA}$, and $EW(\text{Li I}) < 0.4 \text{ \AA}$, *candidate* weak-line T Tauri stars (WTTS) (cf. Tachihara et al. 2005). Earlier (G and K) spectral types need lower $EW(H\alpha)$ for the CTTS classification. Our input list contains a few A- and F-type stars, whose candidate PMS status is based on their IRAS associations and which display H α in absorption, but $EW(H\alpha)$ is lower than the value characteristic of the spectral type, suggesting that the photospheric absorption is partly filled by emission. We regard these stars candidate Herbig Ae stars. According to the above criteria, 77 of the observed 170 stars have shown spectra characteristic of pre-main sequence stars. These stars are listed in Table 1. The observed stars rejected as PMS objects are listed in Table 2. We show examples of non-PMS stars from the candidate list by Kun (1998) in Fig. 1.

The spectra of the stars listed in Table 1 are shown in Figs. 2–4. Figure 2 shows the spectra of the PMS stars, normalized to the continua, observed with CAFOS+R–100. Fig. 3 shows those observed with CAFOS+G–100. The FAST spectra of stars classified as PMS objects, normalized to the value of the continuum at 6560 \AA , are shown in Fig. 4. The insets show the shape of the H α line in more detail, i.e. the section of the spectrum between 6545 and 6580 \AA . The vertical size of the enlarged section is scaled to the peak intensity of the line.

Results of the spectroscopic observations are presented in Tables 3 and 4. The instruments of observation, the derived spectral types, the type of the H α emission line shape, according to the scheme introduced by Reipurth, Pedrosa & Lago (1996), and a list of further emission lines identified in the spectra are listed in Table 3. We show in Table 4 the equivalent widths of the H α , Li I, and Ca II infrared triplet lines in \AA , as well as $\Delta v(10\%)$, the width of the H α line 10% above the continuum, deconvolved by the response of the instrument, in km s^{-1} . Whereas Li I is an important indicator of youth, $EW(H\alpha)$, $EW(\text{Ca II } 8542)$, and $\Delta v(10\%)$ are used as accretion indicators (Muzerolle et al. 1998; Natta et al. 2004; Dahm 2008). The equivalent widths were determined by fitting a Gaussian or multiple Gaussians to the lines using the IRAF task ‘splot’. The uncertainties, derived from repeated measurements, are about 10%. The real uncertainties of the Li I equivalent widths may be higher due to the blending of the line with neighboring Fe I lines (at 6703.5, 6705.1, 6707.4, and 6710.3 \AA). We used the ‘deblend’ command of the ‘splot’ task of IRAF to separate the Li I line from the Ca I λ 6718 and [S II] λ 6717 lines. The last column of Table 4 shows the PMS type of the object, based on our data.

2.3. BVR_CI_C photometry

Photometric observations in the BVR_CI_C bands of the young stars identified by our spectroscopic observations were undertaken during one night in 2004 December, two nights in 2005 June, and eight nights in 2006 September and October using the 1-m RCC-telescope of the Konkoly Observatory. We used a Princeton Instruments VersArray:1300B camera, that utilizes a back-illuminated, 1300×1340 pixel Roper Scientific CCD. The pixel size is $20 \mu\text{m}$, corresponding to 0.31 arcsec on the sky. Integration times were between 30 s and 600 s. To calibrate the photometry we observed the open cluster NGC 7790 several times each night, at various airmasses, as well as NGC 188 once each night. We reduced the images in IRAF. After bias subtraction and flatfield correction PSF-photometry was performed using the ‘daophot’ package. The field of view, 6.7×6.9 arcmin, contained several stars suitable for establishing the point spread function of the images. The transformation formulae between the instrumental and standard magnitudes and color indices as a function of the airmass were established each night by measuring the instrumental magnitudes of some 80 photometric standard stars published by Stetson (2000) for NGC 7790 and 40 stars in NGC 188. Each target was observed at least twice, on two different nights, and several stars on three or more nights. The photometric errors, obtained as quadratic sums of the formal errors of the instrumental magnitudes and those of the coefficients of the transformation equations are about ± 0.02 mag for stars brighter than about 16th mag, and about ± 0.05 mag for the fainter stars.

The results of the photometry are presented in Table 5. The magnitudes listed are averages of 2–4 independent measurements. In several cases magnitude differences well above the formal errors, indicative of variability, were detected. We show in parentheses the mean absolute deviation of the magnitudes, and indicate the variability in Col. 6. During the psf photometry faint visual companions were revealed near some objects. We designate these stars in Table 5 by adding a letter to the name of the primary, and give the angular distance from the primary and the position angle in Col. 6 of Table 5. Figure 5 shows the I_C images of the visual double stars observed.

2.4. Infrared archive data

We supplemented our observational data with the near infrared data of the 2MASS All Sky Catalog (Cutri et al. 2003) and the far-infrared data of the IRAS PSC (IPAC 1988) and FSC (Moshir et al. 1990). One of the target stars, LkH α 425, is not included in the 2MASS point source catalog. A nonstellar object (artifact?) appears in the 2MASS images next to this star. We took JHK photometric data for this star from Sellgren (1983).

Spitzer IRAC and MIPS fluxes are available for parts of L 1228 and L 1251, as well as for

RNO 124 and RNO 129 in the c2d data archive (Evans et al. 2003)². NGC 7129 was observed by IRAC and MIPS as part of the Spitzer young stellar cluster survey (Gutermuth et al. 2009). Four cluster members included in the Spitzer survey are common with our targets. The magnitudes of these stars are listed in Table 4 of Gutermuth et al. (2009). IRAC and MIPS photometric data for NGC 7023 are presented in Kirk et al. (2009). All of our program stars in NGC 7023 but SX Cep are included in their Table 6. The identifiers of our stars in both papers are shown in Col. 4 of Table 1.

To obtain IRAC and MIPS 24 μm photometric data for SX Cep we downloaded the basic calibrated data (BCD) frames processed with the SSC IRAC Pipeline v14.0 for Prog ID 30574 and created mosaics from the BCD frames using a custom IDL program. For details see Gutermuth et al. (2008). Aperture photometry was carried out using PhotVis version 1.10 which is an IDL-GUI based photometry visualization tool. See Gutermuth et al. (2004) for further details on PhotVis. The radii of the source aperture, and of the inner and outer boundaries of the sky annulus were 2.4, 2.4 and 7.2 arc-second respectively. For MIPS the frames were processed using the MIPS Data Analysis Tool (Gordon et al. 2005). PSF fitting in the IRAF/DAOPHOT package was used to obtain the following photometry for SX Cep: $[3.6] = 8.91 \pm 0.01$, $[4.5] = 8.65 \pm 0.02$, $[5.8] = 8.24 \pm 0.06$, $[8.0] = 7.66 \pm 0.04$, $[24] = 5.85 \pm 0.07$.

3. Results

3.1. Visual binaries, spectroscopic and photometric variability

Figure 5 shows the I_C images of the visual double stars detected during our observations. Photometry was performed separately for the components, whereas we observed only the spectrum of the brighter component of FT Cep, NGC 7023 RS 5, OSHA 50, [K98c] Em* 46, NGC 7129 SV3, [K98c] Em* 95, and AS 507. The uncertainty ellipse of IRAS 22152+6947 contained two nearly equally bright stars separated by $4''$. The eastern component is a G2 dwarf, while the western component is an F5 star with weak $H\alpha$ emission. We include the F5 star in our final list of PMS stars. Our observations find RNO 129, OSHA 48, LkH α 428, and [K98c] Em* 119 to be new binary T Tauri stars.

Variability of several stars has already been established (e.g. Rosino & Romano 1962; Shevchenko & Yakubov 1989; Grankin et al. 2007). We observed strong night-to-night variation of FT Cep and most of the stars in L 1251. Spectra of some stars were observed at more than one epoch, and significant variations were found in the equivalent width of the $H\alpha$ line in some cases. Figure 6 shows the three most conspicuous cases.

²http://data.spitzer.caltech.edu/popular/c2d/20071101_enhanced_v1/

3.2. Surface distribution of the PMS stars

Figure 7 shows the distribution of the PMS stars overplotted on the extinction map of the region published by Dobashi et al. (2005). In addition to our target stars, known Class I objects, Herbig Ae/Be stars and WTTSs are also indicated. Dotted lines indicate the nominal boundaries of the Cepheus flare Shell (Olano et al. 2006), a section of Loop III, and the far-infrared loop G 109+11 (Kiss et al. 2004). The dashed line shows a section of the Cepheus Bubble, located at some 800 pc, and possibly associated with NGC 7129 (Ábrahám et al. 2000). For better visibility, parts of the map centered on NGC 7023, L 1228, L 1251, and NGC 7129 are shown enlarged in Figs. 8–11.

The clusters of young stars are concentrated near the edges of the cloud complex, and avoid the central part of the region. All known star forming clouds but L 1221 are associated with optically visible young stars. L 1172/L 1174 displays head–tail structure, with the optically visible cluster in the head, indicative of star formation propagating from higher towards lower Galactic longitudes. The 13 stars associated with L 1228 (Fig. 9) apparently belong to three small aggregates: L 1228 S (Padgett et al. 2004), L 1228 A (Bally et al. 1995), and RNO 129 (Movsessian & Magakian 2004). Most of the young stars of L 1251 form two small clusters, associated with two dense $C^{18}O$ cores, L 1251 C and L 1251 E (Sato et al. 1994). On-going star formation has been observed in both cores (e.g. Beltrán et al. 2001; Reipurth et al. 2004; Lee et al. 2006, 2007; Kirk et al. 2009). The strong X-ray source [KP93] 2-43 (Simon 2006) is projected on a lower density part of the cloud between the two cores. The cometary shape of L 1251, and the presence of three PMS stars on its high longitude side suggest star formation propagating from the higher towards the lower Galactic longitudes. Two CTTSs and a WTTS are projected near L 1261. The extinction map of the NGC 7129 region, displayed in Fig. 11 shows that its associated cloud, L 1181 contains two star-forming clumps. The cluster is embedded in the low-latitude clump, whereas V391 Cep and four newly confirmed CTTSs (NGC 7129 SV1–V3, and [K98c] Em* 72) are associated with another clump at the high-latitude part of the cloud.

In addition to the clusters associated with known star-forming clouds, PMS stars can be found widely scattered at the low-latitude side of the region, between L 1177 and L 1219, apparently along the periphery and inside of the shell G 109+11. A small group can be seen close to L 1235 and SV Cep. The A1 type $H\alpha$ emission star coinciding with IRAS 22219+7901 (TYC 4608-2063-1), and a group of WTTSs are projected on the cleared central region of the CFS.

3.3. Line-of-sight distribution of the PMS stars

Various distance values can be found in the literature for the star forming clouds of the Cepheus flare. A comprehensive table of published distance estimates is presented in Table 3 of Kun et al. (2008). We adopt the distances for the clouds and the associated PMS stars listed in Table 6.

The distances of PMS stars far from the known star forming clouds require further considera-

tion. A small aggregate can be found around $l \approx 106^\circ$, $b \approx +13.6^\circ$, close to the star forming cloud L 1177. The members of this group are [K98c] Em* 53, [K98c] Em* 58, 2MASS 21225427+6921345, the H Ae star BD +68°1118, and a candidate PMS star, 2MASS 21223461+6921142. We estimated the distance of this aggregate by the assumption that BD +68°1118 is a member and lies on the ZAMS. This assumption results in a distance of 390 pc. The star BD +67°1300 (VDB 141) illuminates part of the L 1177 dark cloud (see Fig. 12), and provides us another distance estimate. Our FAST spectrum for BD +67°1300 indicates a spectral type of K0III. The absolute magnitudes of K0 giants, tabulated by Wainscoat et al. (1992), together with the photometric data of BD +67°1300 and its associated 2MASS source, found in the NOMAD³ catalogue, result in a distance $D \approx 370$ pc. The large dispersion of the absolute magnitudes of K giants, $\sigma_M = 0.7$ (Wainscoat et al. 1992), corresponds to a 1σ range of distances of $270 \text{ pc} \lesssim D \lesssim 515 \text{ pc}$. We derive the luminosities of the stars near L 1177 using a distance of 390 pc. This value is close to the distance of L 1219/B 175, surrounded by a group of PMS stars (BH Cep, BO Cep, IRAS 22129+6949, IRAS F22144+6923, IRAS 22152+6947, [K98c] Em* 119, [TNK2005] 37 (Tachihara et al. 2005)). We assume that these stars are associated with L 1219 at ~ 400 pc. The candidate PMS star 2MASS 22283821+7119023 is probably a further member of this group. Both L 1177 and L 1219 are bordered by a high density rim on the low-latitude side (cf. Bally & Reipurth 2001, see also Fig. 12), indicative of shocks propagating from the direction of low Galactic latitudes. Their similar morphologies and distances suggest that both clouds and the associated star formation may be influenced by the large Galactic shell G 109+11 (Kiss et al. 2004). Therefore we refer to this group of PMS stars as the *G 109+11 association*.

Another small aggregate ([K98c] Em* 95, 108, and 109) can be seen projected near the H Ae star SV Cep, and at the same time close to the head of the starless dark cloud L 1235. Whereas L 1235 is situated at 300 pc (Kun et al. 2008), SV Cep is much more distant (715 pc: Friedemann et al. 1992; 700 ± 70 pc: Kun et al. 2000; 596_{-43}^{+106} pc: Montesinos et al. 2009). Plotting these stars in the HRD with a distance of 300 pc, we obtain ages between 10 and 20 million years, inconsistent with typical CTTSs. Assuming that the stars are as distant as SV Cep (600 pc), we estimate ages of 1–5 Myr, similar to that of SV Cep (Montesinos et al. 2009). Therefore we assume that these stars formed in the same cloud as SV Cep.

We assume that the apparently isolated stars IRAS 20535+7439 and RNO 135 belong to the cloud complex at 300 pc, and [K98c] Em* 73 is a member of the G 109+11 association at 400-pc. We have no guideline for finding the distance and luminosity of IRAS 22219+7901. If we assume that it is a main sequence star, we estimate a distance of 1.3 kpc.

³<http://www.nofs.navy.mil/nomad>

3.4. Interstellar extinction and luminosities

We derived the interstellar extinction suffered by the program stars from their $E_{R_C-I_C}$ and E_{I_C-J} color excesses. The unreddened color indices of the spectral types were adopted from Kenyon & Hartmann (1995). We determined A_V from both color excesses independently, using Cardelli et al.’s (1989) extinction law with $R_V = 3.1$, and then accepted the average of both values as the visual extinction of the star. For visual binaries that are resolved in our optical images, but unresolved in 2MASS, we used only $E_{R_C-I_C}$ to determine A_V . We corrected the observed magnitudes using the $A(\lambda)/A_V$ relations according to the same extinction law. The extinction law with $R_V = 3.1$ proved inadequate in the case of the most heavily reddened stars, above $A_V \approx 4$ mag: the unreddened SEDs of these stars over the $V-J$ region poorly fitted the shape of the photospheric SED. Therefore we rederived the extinctions of these stars using $R_V = 5.5$, using the relations $A(\lambda)/A_V$ given by Cardelli et al. (1989). $R_V = 3.1$ gave definitely better results for most of the lightly reddened stars: for instance, in L 1251 we used $R_V = 5.5$ for [KP93] 2-1, 46, [KP93] 3-10, [RD95] A, [RD95] B, and [ETM94] Star 3, and $R_V = 3.1$ for the other members. Exceptions are the apparently lightly reddened stars associated with small reflection nebulae or exhibiting Class I SEDs, namely NGC 7023 RS 10, [K98c] Em*58, and [K98c] Em*119. The apparently low reddening of these stars results from the contribution of scattered light to their color indices. We corrected their fluxes for the extinction using $R_V = 5.5$. The difference between the two A_V values, derived from $E_{R_C-I_C}$ and E_{I_C-J} , allowed us to estimate the uncertainty as ± 0.5 mag. Bolometric magnitudes were derived by applying the bolometric corrections, BC_{I_C} , tabulated by Hartigan et al. (1994). Effective temperatures of the spectral types were adopted from Kenyon & Hartmann (1995). Luminosities were derived using the distances listed in Table 6. The T_{eff} and L_{bol} values are listed in Table 7.

3.5. Hertzsprung–Russell diagrams

The Hertzsprung–Russell diagrams of the pre-main sequence stars are plotted in Figs. 13–17, separately for L 1228, NGC 7023, L 1251, and NGC 7129. The G 109+11 association, the stars associated with L 1155/L 1157, SV Cep, and L 1261, as well as the isolated stars IRAS 20535+7439 and RNO 135 are plotted with varied symbols in Fig. 17. Since we could not find absorption features suitable for spectral classification in the spectrum of PV Cep, we accepted a spectral type of K0, reported by Magakian & Movsessian (2001). Evolutionary tracks and isochrones, as well as the position of the birthline and zero-age main-sequence (Palla & Stahler 1999) are also shown. Masses and ages, derived from these diagrams, are listed in Table 7.

3.6. Accretion signatures

Both the emission spectra and the shape of the SED carry information on the mass accretion rate from the disk onto the star. The accretion rates \dot{M}_{acc} of our PMS stars were estimated from the H α line width $\Delta v(\text{H}\alpha)$ using the formula of Natta et al. (2004), and from the H α and Ca II luminosities using the formulae of Dahm (2008). Since our spectra are not flux calibrated, we derived the emission line luminosities from the equivalent widths, using the extinction-corrected R_C and I_C magnitudes for determining the underlying stellar flux for the H α and Ca II lines, respectively. In order to convert the luminosity to accretion rate according to the relationship

$$L_{\text{acc}} \approx \frac{G\dot{M}M_*}{R_*} \left(1 - \frac{R_*}{R_0}\right) \quad (1)$$

we took the stellar mass, M_* , and radius, R_* from the HRD, and adopted $R_0 \approx 5 R_*$ for the inner radius of the gaseous disk (Gullbring et al. 1998). The accretion rates, \dot{M}_{acc} , obtained from the H α and Ca II 8542 Å lines are listed in Table 7.

Figure 18 shows the relationship between the accretion rates, \dot{M}_{acc} , resulted from $\Delta v(\text{H}\alpha)$ and $L(\text{H}\alpha)$, respectively. Given the empirical nature of both relationships the large scatter is not surprising. An additional source of uncertainty of the results is that our spectroscopic and photometric observations were obtained at different epochs. We notice that for stars exhibiting double-peaked H α emission line accretion rates derived from $\Delta v(\text{H}\alpha)$ are systematically larger than those derived from $L(\text{H}\alpha)$. Double-peaked H α lines (Types II and III in Table 3) have among the strongest emission lines in the sample. All but one ([K98c] Em* 109) belong to the types IIB or IIIB, i.e. the absorption dip is on the blue side of the main peak, indicating the contribution of wind to the line shape. A reason for the discrepancy may be that, due to the absorption by the wind, the peak of the H α emission is lower than it would be without the contribution of wind. Thus the effects of the wind are a smaller equivalent width and, since the 10% level of the peak is also lower, a larger line width at this level. We also note that the H α lines of these stars are wider than those used by Natta et al. (2004) for calibrating the \dot{M}_{acc} vs. $\Delta v(\text{H}\alpha)$ relationship. Accretion rates derived from $L(\text{H}\alpha)$ and $L(8542)$ are consistent with each other according to Fig. 19. We note, however, that there is a large scatter in \dot{M} from Ca II at fixed \dot{M} from H α , thus we cannot state that there is a 1:1 relation between them.

We examined the dependence of accretion rate on stellar mass. Figure 20 shows the result. The accretion rates plotted are averages of both methods derived from the H α emission line. The line fitted to the data is $\log \dot{M}_{\text{acc}} \propto 1.74 \times \log M_*$, compatible with similar relationships found for other nearby star forming regions ($\log \dot{M}_{\text{acc}} \propto 1.8 \times \log M_*$; Natta et al. 2006; Herczeg & Hillenbrand 2008). The correlation, however, is rather weak: the Pearson correlation coefficient is 0.48. The large scatter of this plot (exceeding three orders of magnitude at a fixed M_*) partly originates from plotting together stars of several regions, having different ages and accretion histories. For instance, most of the (older) dispersed stars appear below the fitted line, whereas the stars of L 1251 show

higher accretion rates than the average. However, no clear dependence of \dot{M}_{acc} on the stellar age can be found in our data set. As Tilling et al. (2008) pointed out, biases are hard to remove in quantifying the \dot{M}_{acc} vs. M_* relation.

3.7. Spectral energy distributions

The optical, near- and mid-infrared parts of the spectral energy distributions (SEDs) of the programme stars were constructed using all available photometric data, each corrected for the interstellar extinction. The fluxes corresponding to zero magnitude were obtained from Glass (1999) for the VR_CI_C bands, and from the 2MASS All Sky Data release web document⁴ for the JHK_s bands. IRAS fluxes are also plotted when available. IRAS fluxes of 2MASS 21225427+6921345 were obtained by Scanpi⁵. The resulting SEDs are shown in Figs. 21–25, separately for the clusters/aggregates of the region. Photospheric SEDs have been drawn by dashed lines. Their values were determined from the dereddened I_C magnitudes, and from the color indices corresponding to the spectral types. We also plotted for comparison the median SED of the T Tauri stars of the Taurus star forming region (D’Alessio et al. 1999), the best-studied sample population of 1–2 Myr old low-mass stars.

The shape of the SED allows us a qualitative classification of the circumstellar environment of the young stars. According to the slope between 2 and 24 μm , $\alpha_{24-K} = d \log(\lambda F_\lambda) / d \log(\lambda)$, Class I ($\alpha > 0.3$), Flat ($0.3 > \alpha > -0.3$), Class II ($-0.3 > \alpha > -1.6$), and Class III ($\alpha < -1.6$) YSOs are distinguished (Lada 1991; Evans et al. 2009). Class I infrared sources are probably among the youngest PMS stars, close to the end of the main accretion phase of their evolution. Their circumstellar environment is composed of a disk and an envelope. Class II sources are CTTSs surrounded by optically thick accretion disks, and the low infrared excesses of Class III stars originate from optically thin disks.

Four stars, namely PV Cep, NGC 7023 RS 10, [K98c] Em* 58, and GGD 33a exhibit SEDs characteristic of Class I objects. The luminosities of these stars, derived from the optical observations, are very low, indicating that we observe the light of these stars scattered from edge-on disk or envelope. The underestimated luminosity is also reflected in the discrepancy between the accretion rates obtained from $\Delta v(\text{H}\alpha)$ and $L(\text{H}\alpha)$. PV Cep and GGD 33a are associated with Herbig–Harro objects (Gómez, Whitney, & Kenyon 1997; Eiroa, Gómez de Castro, & Miranda 1992), suggesting that they are probably real Class I objects, embedded in massive envelopes. The small reflection nebula associated with NGC 7023 RS 10 may also be an indicator of the envelope. The nature of [K98c] Em* 58 is uncertain. It may either be an edge-on disk or an unresolved binary system. The histogram of α_{24-K} for our stars is shown in the left panel of Fig. 26. Five percent of the studied

⁴http://www.ipac.caltech.edu/2mass/releases/allsky/doc/sec6_4a.html

⁵<http://scanpiops.ipac.caltech.edu:9000/applications/Scanpi/index.html>

stars belong to the Class I, 13% exhibit Flat SEDs, 60% are Class II, 3% Class III, and 18% (14 stars) remain unclassified due to the lack of both 24 and 25 μm fluxes.

Cieza et al. (2007) introduced a two-dimensional way of classification of SEDs, based on λ_{turnoff} , the longest wavelength at which the observed SED is photospheric, and α_{excess} , the slope of the SED for $\lambda > \lambda_{\text{turnoff}}$. $\lambda_{\text{turnoff}} \lesssim 2 \mu\text{m}$ may indicate accreting stars, with the inner edge of the disk at the dust sublimation radius. SEDs with λ_{turnoff} in the IRAC wavelength range may result from more evolved, purely irradiated disks with inner holes. The right panel of Fig. 26 shows the histogram of λ_{turnoff} for our target stars. We found $\lambda_{\text{turnoff}} \leq 2 \mu\text{m}$ for some 45% of the studied objects, while λ_{turnoff} cannot be determined for 22% due to the lack of IRAC data. These stars obviously have $\lambda_{\text{turnoff}} > 2 \mu\text{m}$. Thus slightly less than half of our studied stars exhibit near-infrared excesses. Remarkably SEDs of various shape (cf. Evans et al. 2009) occur in each small cluster of the region. For instance, we find both Flat SEDs (KP93 2-2) and transitional/annular disks (KP93 2-3) in L 1251, and both Class I (NGC 7023 RS 10) and purely photospheric (HZ Cep) SEDs in NGC 7023. On the contrary, the seven observed SEDs of L 1228 S are less diverse: none of them show NIR excess, indicating either evolved disks, or star forming conditions different from those in the other parts of the region.

4. Discussion

4.1. Distribution of stellar and disk properties

Figure 27 shows the histogram of the effective temperatures and masses, derived from the HRD, and mass accretion rates, derived from the H α line (average from both methods). It is apparent that due to the magnitude limit of our observations spectral types later than about M2, and masses lower than about $0.2 M_{\odot}$ are largely missing from our sample. Comparison of the mass distribution with the shape of the Salpeter IMF shows that the incompleteness of our sample starts at around $0.5 M_{\odot}$. The median mass of the observed stars is $0.8 M_{\odot}$. The median accretion rate for our sample, derived from the H α emission line, is $\dot{M}_{\text{acc}} = 3.6 \times 10^{-8} M_{\odot}/\text{yr}$. Gullbring et al. (1998) measured a median accretion rate of $9.6 \times 10^{-9} M_{\odot}/\text{yr}$ for 17 CTTSs in Taurus, and Natta et al. (2006) measured a median accretion rate of $4.4 \times 10^{-9} M_{\odot}/\text{yr}$ for 43 members of ρ Oph (upper limits excluded). These figures show that our target selection resulted in a limited interval of effective temperatures and masses, and in the detection of the most actively accreting members of the population. Median stellar parameters, as well as median α_{24-K} and λ_{turnoff} for various parts of the Cepheus flare are summarized in Table 8.

4.2. A possible origin of star formation in the Cepheus flare

The CFS/Loop III system may represent a link between the apparently distinct star forming clouds (Olano et al. 2006; Kun 2007). L 1147/L 1158 and NGC 7023 are located outside the CFS, but close to the periphery of Loop III. The giant, nearly concentric shells are suggestive that multiple supernova explosions occurred inside the Cepheus void, that is, the presence of OB stars there in the past few million years. Looking for the remnants of such an association we find the small R-association consisting of the classical Cepheid SU Cas and a small group of A and B type stars at a distance of 258 pc (Turner & Evans 1984). We have no sufficient data for deciding whether this small group is a remnant of a large OB association. The G 109+11 association at 400-pc may result from a star formation event due to the impact of the shell G 109+11 6–7 million years ago. The expansion of the shell towards higher latitudes might have triggered star formation in L 1177. The 50-Myr old association Cep OB6 at a distance of 300 pc and towards low-latitudes from the Cepheus flare may be the source of the shell (Bally & Reipurth 2001).

5. Conclusions

From spectroscopic and photometric observations, we estimated the effective temperatures and luminosities of 78 PMS stars in the Cepheus flare region, 65 of which are newly confirmed PMS stars. Comparing the results with pre-main sequence evolutionary models we estimate stellar masses of 0.2–2.4 M_{\odot} and stellar ages of 0.1–15 Myr. From archival IRAS, 2MASS, and Spitzer data, we constructed the spectral energy distributions; 5% of the stars are Class I, 5% Flat, 81% Class II, and 9% Class III.

Star forming clouds and PMS stars of the region belong to the complexes as follows.

- Star formation associated with the large expanding system of Cepheus flare Shell/Loop III occurs in the clouds L 1148/L 1158, L 1172/L 1174, L 1251, L 1228 and L 1261/L 1262. The latter two clouds are located on the approaching side of the expanding shell.
- A sparse association consisting of 6–7 Myr old PMS stars at the low-latitude part of the region ($105^{\circ} \lesssim l \lesssim 112^{\circ}$, $10^{\circ} \lesssim b \lesssim 14^{\circ}$) can be found at a distance of 380–400 pc. The shapes of the clouds in this part of the region suggest shocks from the direction of the Galactic plane.
- Low-mass PMS stars are associated with the Herbig Ae star SV Cep, located at ~ 600 pc.
- NGC 7129, at ~ 800 pc from the Sun, is probably associated with the Cepheus Bubble, created by the older subgroup of the association Cep OB2. Stars have been formed in at least two clumps of its natal cloud L 1181.

The A1-type $H\alpha$ emission star associated with IRAS 22219+7901 is probably more distant than the Cepheus flare clouds. Its nature remains uncertain.

Our results are partly based on observations obtained at the Centro Astronómico Hispano Alemán (CAHA) at Calar Alto, operated jointly by the Max-Planck-Institut für Astronomie and the Instituto de Astrofísica de Andalucía (CSIC). We thank Calar Alto Observatory for allocation of director's discretionary time to this programme. This publication makes use of data products from the Two Micron All Sky Survey, which is a joint project of the University of Massachusetts and the Infrared Processing and Analysis Center/California Institute of Technology, funded by the National Aeronautics and Space Administration and the National Science Foundation. This work makes use of observations made with the *Spitzer Space Telescope*, which is operated by the Jet Propulsion Laboratory, California Institute of Technology under a contract with NASA. Our observations were supported by the OPTICON. OPTICON has received research funding from the European Community's Sixth Framework Programme under contract number RII3-CT-001566. This research was supported by the Hungarian OTKA grant T49082. Support for Z. Balog was provided by NASA through contract 1255094, issued by JPL/Caltech. We are grateful to László Szabados for careful reading of the manuscript.

REFERENCES

- Ábrahám, P., Balázs, L. G., & Kun, M. 2000, *A&A*, 354, 645
- Balázs, L. G., Ábrahám, P., Kun, M., et al. 2004, *A&A*, 425, 133
- Bally, J., Devine, D., Fesen, R. A., & Lane, A. P. 1995, *ApJ*, 454, 345
- Bally, J., & Reipurth, B. 2001, *ApJ*, 552, L159
- Balog, Z., & Kenyon, S. J. 2002, *AJ*, 124, 2083
- Barrado y Navascués, D., & Martín, E. L. 2003, *AJ*, 126, 2997
- Beltrán, M. T., Estalella, R., Anglada, G., et al. 2001, *AJ*, 121, 1156
- Berkhuijsen, E. M. 1973, *A&A*, 24, 143
- Le Borgne, J.-F., Bruzual, G., Pello, R., et al. 2003, *A&A*, 402, 433
- Cardelli, J. A., Clayton, G. C., & Mathis, J. S. 1989, *ApJ*, 345, 245
- Cieza, L., Padgett, D. L., Stapelfeldt, K. R. et al. 2007, *ApJ*, 667, 308
- Clemens, D. P., & Barvainis, R. 1988, *ApJS*, 68, 257
- Cohen, M., & Kuhl, L. V. 1979, *ApJS*, 41, 743
- Cutri, R. M., Skrutskie, M. F. van Dyk, S. et al. 2003, *VizieR On-line Data Catalog: II/246*
- Dahm, S. E. 2008, *AJ*, 136, 521

- D'Alessio, P., Calvet, N., Hartmann, L., et al. 1999, *ApJ*, 527, 893
- Dobashi, K., Uehara, H., Kandori, R., et al. 2005, *PASJ*, 57, S1
- Dullemond, C. P., Natta, A., & Testi, L. 2006, *ApJ*, 645, L69
- Eiroa, C., Gómez de Castro, A. I., & Miranda, L. F. 1992, *A&AS*, 92, 721
- Eiroa, C., Torrelles, J. M., Miranda, L. F., Anglada, G., & Estalella, R. 1994, *A&AS*, 108, 73
- Eredics, M., & Kun, M. 2003, *Comm. Konkoly Obs.*, 13, 27
- Evans, N., Calvet, N., Cieza, L. et al. 2009, arXiv:0901.1691
- Evans, N. J., II, Allen, L. E., Blake, G. A., et al. 2003, *PASP*, 115, 965
- Fabricant, D., Cheimets, P., Caldwell, N., & Geary, J. 1998, *PASP*, 110, 79
- Friedemann, C., Reimann, H.-G., & Gürtler, J. 1992, *A&A*, 255, 246
- Glass, I. S. 1999, *Handbook of Infrared Astronomy*, Cambridge Univ. Press, p. 63
- Gómez, M., Whitney, B. A., & Kenyon, S. J. 1997, *AJ*, 114, 1138
- Gordon, K. D., et al. 2005, *PASP*, 117, 503
- Grankin, K. N., Melnikov, S. Y., Bouvier, J., et al. 2007, *A&A*, 461, 183
- Grenier, I. A., Lebrun, F., Arnaud, M., Dame, T. M., & Thaddeus, P. 1989, *ApJ*, 347, 231
- Gullbring, E., Hartmann, L., Briceño, C., & Calvet, N. 1998, *ApJ*, 492, 323
- Gutermuth, R. A., Megeath, S. T., Muzerolle, J., et al. 2004, *ApJS*, 154, 374
- Gutermuth, R. A., Myers, P. C., Megeath, S. T. et al. 2008, *ApJ*, 674, 336
- Gutermuth, R. A., Megeath, S. T., Myers, P. C., Allen, L. E., Pipher, J. L., & Fazio, G. G. 2009, *ApJS*, 184, 18
- Hartigan, P., Strom, K. M., & Strom, S. E. 1994, *ApJ*, 427, 961
- Heiles, C. 1967, *ApJS*, 15, 97
- Herbig, G. H., & Bell, K. R. 1988, *Lick Obs. Bull. No. 1111* (Santa Cruz: Lick Obs.)
- Herczeg, G. J., & Hillenbrand, L. A. 2008, *ApJ*, 681, 594
- Hester, J. J., & Desch, S. J. 2005, in: *Chondrites and the Protoplanetary Disk*, Ed. A. N. Krot, E. R. D. Scott, and Bo Reipurth, *ASP Conf. Ser.*, 341, 107

- Hubble, E. 1934, *ApJ*, 79, 8
- Jaschek, C., & Jaschek, M. 1987, *The Classification of Stars*, Cambridge Univ. Press
- Joint IRAS Science W.G. 1988, *IRAS Catalog of Point Sources*, Version 2.0, NASA RP-1190
- Kenyon, S. J., & Hartmann, L. 1995, *ApJS*, 101, 117
- Kirk, J. M., Ward-Thompson, D., Di Francesco, J., Bourke, T. L., Evans II, N. J., et al. 2009, *ApJS*, submitted (arXiv:0903.4063)
- Kirkpatrick, J. D., Henry, T. J., & McCarthy, D. W. 1991, *ApJS*, 77, 417
- Kiss, Cs., Moór, A., & Tóth, L. V. 2004, *A&A*, 418, 131
- Kun, M. 1998, *ApJS*, 115, 59
- Kun, M. 2007, *Proc. IAU Symp. 237, Triggered Star Formation in a Turbulent ISM*, Ed. B. G. Elmegreen and J. Palous, Cambridge Univ. Press, p. 119
- Kun, M., Kiss, Z. T., & Balog, Z. 2008, *Handbook of Star-Forming Regions*, ed. B. Reipurth (San Francisco: ASP), Vol. 1, p. 134
- Kun, M. & Prusti, T. 1993, *A&A*, 272, 235
- Kun, M., Vinkó, J. & Szabados, L. 2000, *MNRAS*, 319, 777
- Lada, C. J. 1991, in: *The Physics of Star Formation and early Stellar Evolution*, eds. C.J. Lada & N. D. Kylafis, Kluwer, p. 329
- Lebrun, F. 1986, *ApJ*, 306, 16
- Lee, J.-E., Di Francesco, J., Lai, S. P. et al. 2006, *ApJ*, 648, 491
- Lee, J.-E., Di Francesco, J., Bourke, T. L., et al. 2007, *ApJ*, 671, 1748
- Lynds, B. T. 1962, *ApJS*, 7, 1
- Magakian, T. Yu. & Movsessian, T. A. 2001, *Astrophysics*, 44, 419
- Magakian, T. Yu., Movsessian, T. A., & Nikogossian, E. H. 2004, *Astrophysics*, 47, 519
- Martín, E. L., & Kun, M. 1996, *A&AS*, 116, 467
- Meehan, L. S. G., Wilking, B. A., Claussen, M. J., et al. 1998, *AJ*, 115, 1599
- Miranda, L. F., Eiroa, C. & Gómez de Castro, A. I. 1993, *A&A*, 271, 564
- Miranda, L. F., Eiroa, C., Fernández, M., & Gómez de Castro, A. I. 1994, *A&A*, 281, 864

- Monnier, J. D., Berger, J.-P., Millan-Gabet, R., et al. 2006, *ApJ*, 644, 444
- Montesinos, B., Eiroa, C., Mora, A., & Merín, B. 2009, *A&A*, 495, 901
- Mora, A., Merín, B., Solano, E., et al. 2001, *A&A*, 378, 116
- Moshir, M., Copan, G., Conrow, T., et al. 1990, *IRAS Faint Source Catalogue*, version 2.0,
- Movsessian, T. A., & Magakian, T. Yu. 2004, *Astron. Rep.*, 48, 988
- Muzerolle, J., Hartmann, L., & Calvet, N. 1998, *AJ*, 116, 453
- Natta, A., Testi, L., Muzerolle, J., et al. 2004, *A&A*, 424, 603
- Natta, A., Testi, L., & Randich, S. 2006, *A&A*, 452, 245
- Ogura, K. & Sato, F. 1990, *PASJ*, 42, 583
- Olano, C. A., Meschin, P. I., & Niemela, V. S. 2006, *MNRAS*, 369, 867
- Padgett, D. L., Rebull, L. M., Noriega-Crespo, A., et al. 2004, *ApJS*, 154, 433
- Page, L., Hinshaw, G., Komatsu, E., et al. 2007, *ApJS*, 170, 335
- Palla, F., & Stahler, S. W. 1999, *ApJ*, 525, 772
- Preibisch, T., Guenther, E., & Zinnecker, H. 2001, *AJ*, 121, 1040
- Racine, R. 1968, *AJ*, 73, 233
- Reipurth, B., Pedrosa, A., & Lago, M. T. V. T. 1996, *A&AS*, 120, 229
- Reipurth, B., Rodríguez, L. F., Anglada, G., & Bally, J. 2004, *AJ*, 127, 1736
- Rosino, L., & Romano, G. 1962, *Asiago Contrib.* 127
- Rosvick, J. M., & Davidge, T. J. 1995, *PASP*, 107, 49
- Sato, F., Mizuno, A., Nagahama, T., et al. 1994, *ApJ*, 435, 279
- Schaefer, B. E. 1986, *ApJ*, 307, 644
- Semkov, E. H. 1993, *IBVS*, 3918
- Sellgren, K. 1983, *AJ*, 88, 985
- Semkov, E. H. 2003, *IBVS*, 5406
- Shevchenko, V. S., & Yakubov, S. D. 1989, *Soviet Ast.*, 33, 370
- Shevchenko, V. S., Ibragimov, M. A., & Yakubov, S. D. 1989, *Soviet Ast.*, 33, 487

- Simon, T. 2006, *AJ*, 131, 501
- Spoelstra, T. A. Th. 1973, *A&A*, 24, 149
- Stetson, P. B. 2000, *PASP*, 112, 925
- Straizys, V., Cernis, K., Kazlauskas, A., & Meistas, E. 1992, *Balt. Astr.*, 1, 149
- Strom, S. E., Vrba, F. J., & Strom, K. M. 1976, *AJ*, 81, 638
- Tachihara, K., Neuhäuser, R., Kun, M., & Fukui Y. 2005, *A&A*, 437, 919
- Taylor, D. K., Dickman, R. L., & Scoville, N. Z. 1987, *ApJ*, 315, 104
- Tilling, I., Clarke, C. J., Pringle, J. E., & Tout, C. A. 2008, *MNRAS*, 385, 1530
- Turner, D. G., & Evans, N. R. 1984, *ApJ*, 283, 254
- Veron-Cetty, M.-P. & Veron, P. 2006, *A&A*, 455, 773
- Wainscoat, R. J., Cohen, M., Volk, K., et al. 1992, *ApJS*, 83, 111
- Yonekura, Y., Dobashi, K., Mizuno, A., et al. 1997, *ApJS*, 110, 21
- Zdanavičius, K., Zdanavičius, J., Straizys, V., & Maskoliunas, M. 2009, *Balt. Astr.*, 18, 33

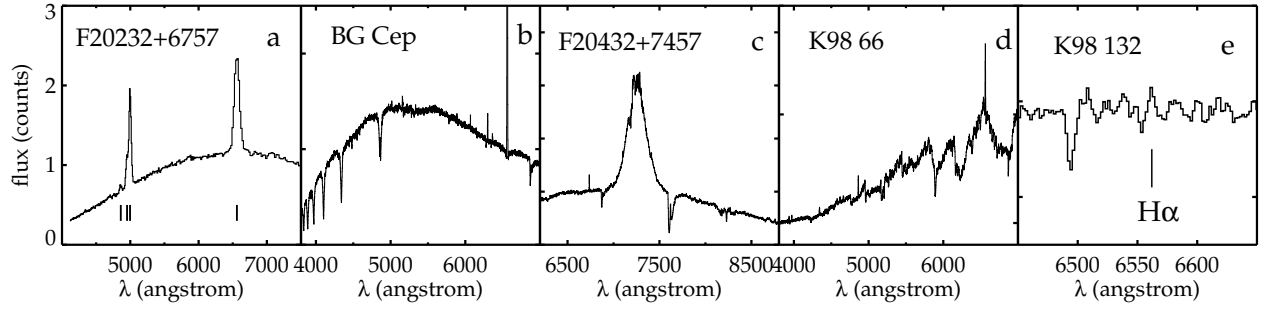


Fig. 1.— Examples of $H\alpha$ emission stars not related to star formation. (a) Objective prism spectrum of the star [K98c] Em* 4, associated with IRAS F20232+6757, taken without red filter. The strong O III emission lines at 4953 and 4996 Å, whose positions are marked along with the $H\alpha$ and $H\beta$, show that this object is a planetary nebula. (b) FAST spectrum of BG Cep, a post-AGB star; (c) CAFOS spectrum of IRAS F20432+7457, which is proved to be a quasar (NED); (d) FAST spectrum of [K98c] Em* 66, an M-type star with Balmer and Ca II H and K line emission but without detectable lithium absorption; (e) part of the spectrum around the $H\alpha$ line of [K98c] Em* 132, which proved to be a non-emission star.

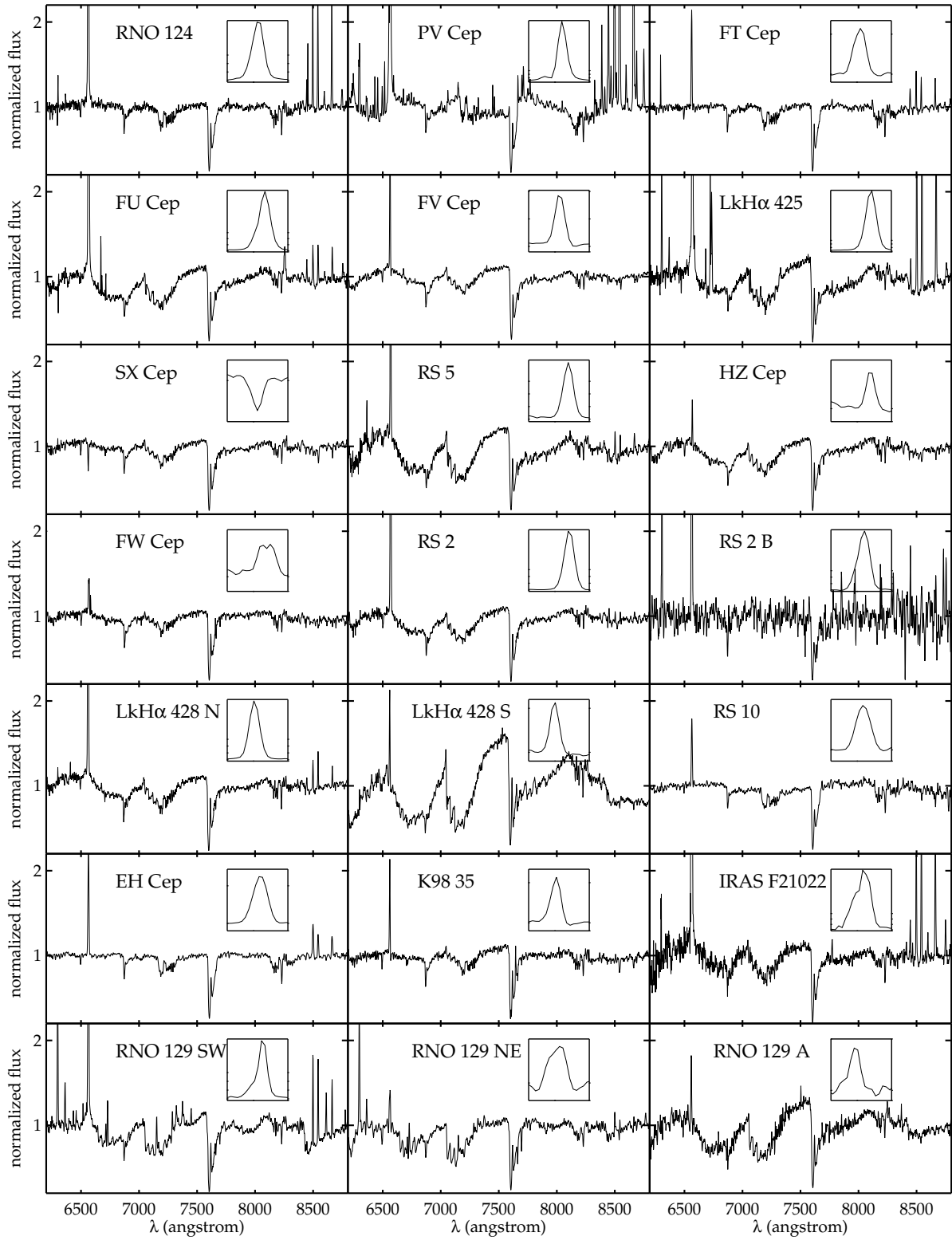


Fig. 2.— Spectra of pre-main sequence stars observed with CAFOS and R-100 grism.

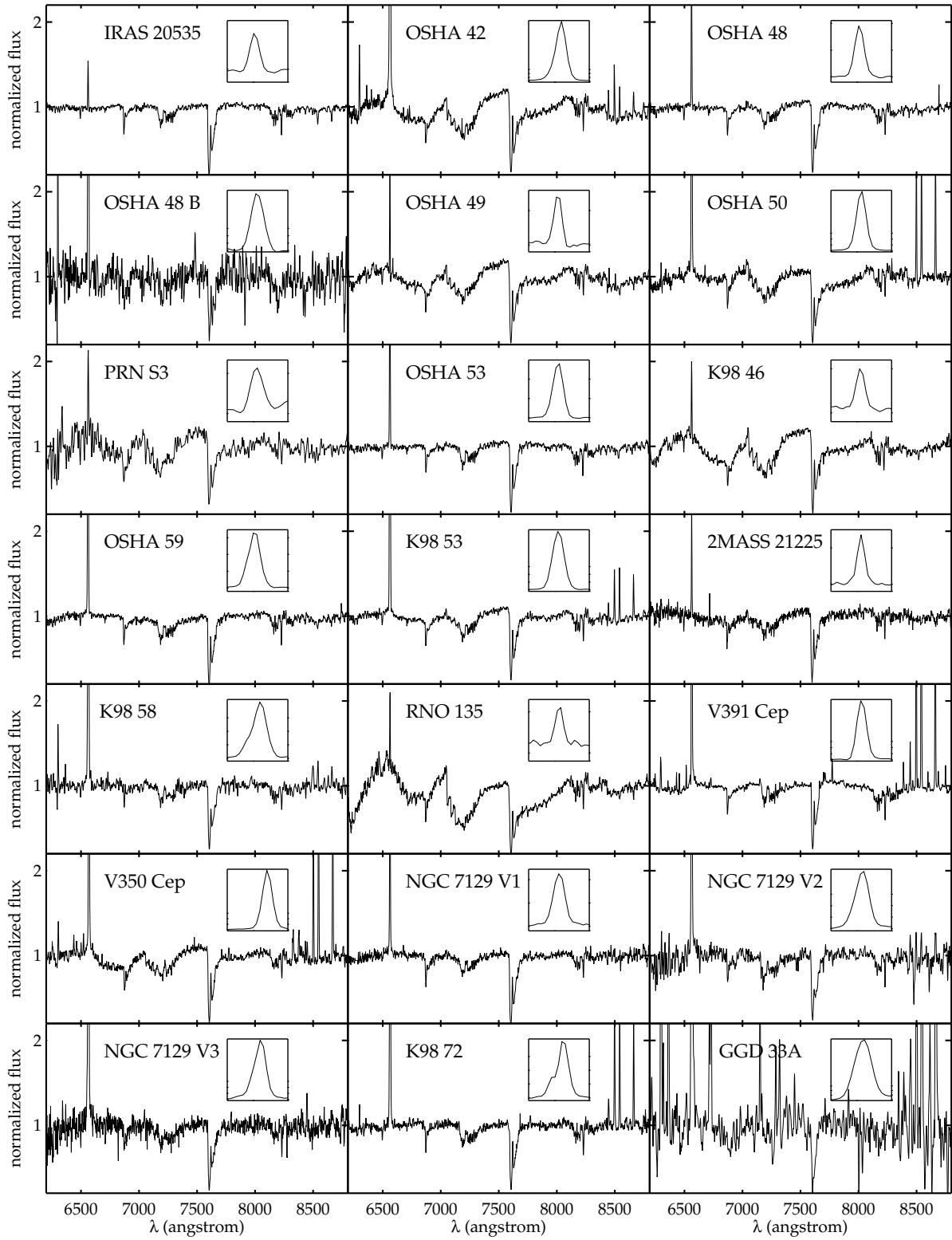


Fig. 2.— Spectra of pre-main sequence stars observed with CAFOS and R-100 grism (continued).

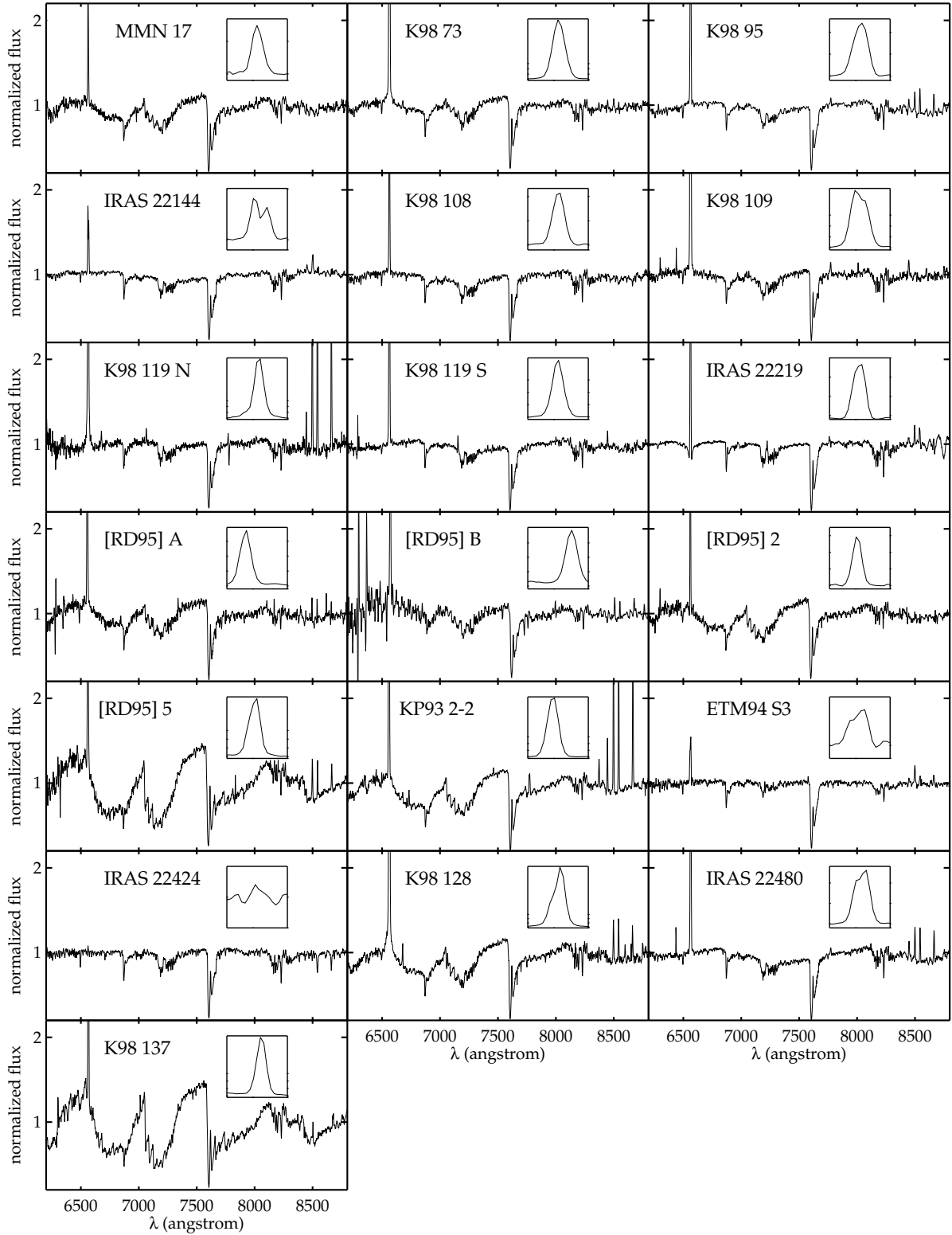


Fig. 2.— Spectra of pre-main sequence stars observed with CAFOS and R-100 grism (continued).

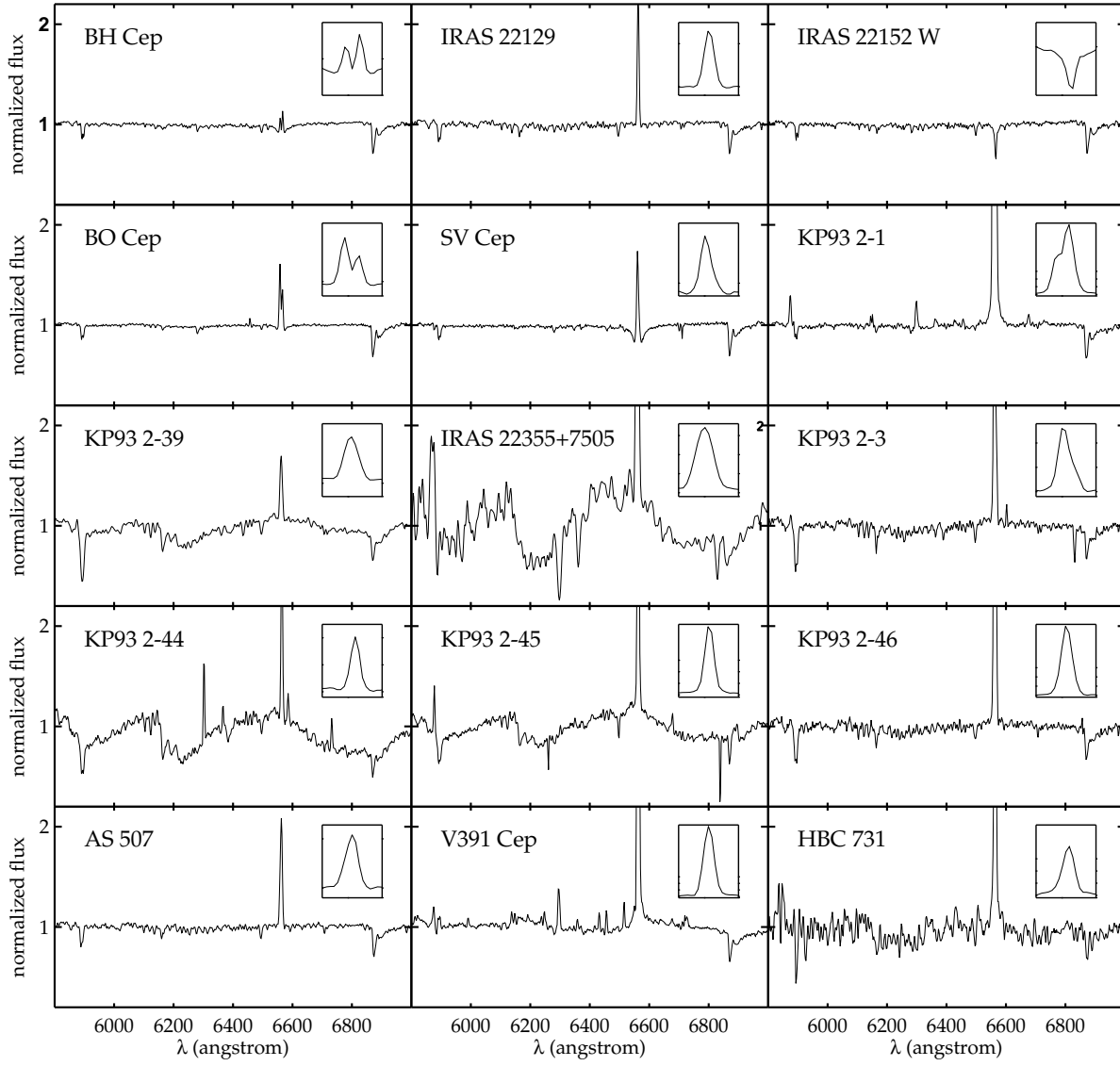


Fig. 3.— Spectra of pre-main sequence stars observed with CAFOS and G-100 grism.

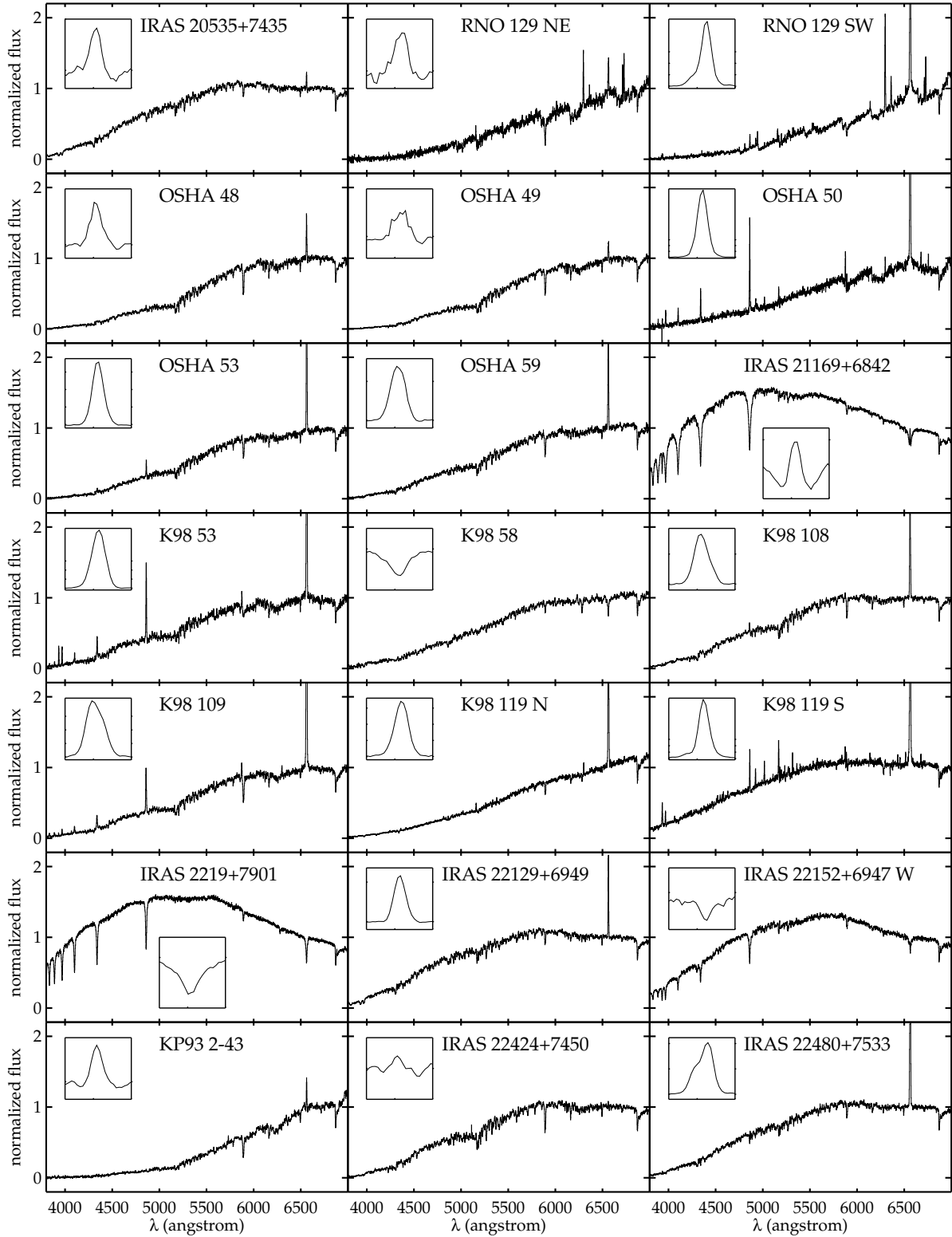


Fig. 4.— Spectra of pre-main sequence stars observed with FAST.

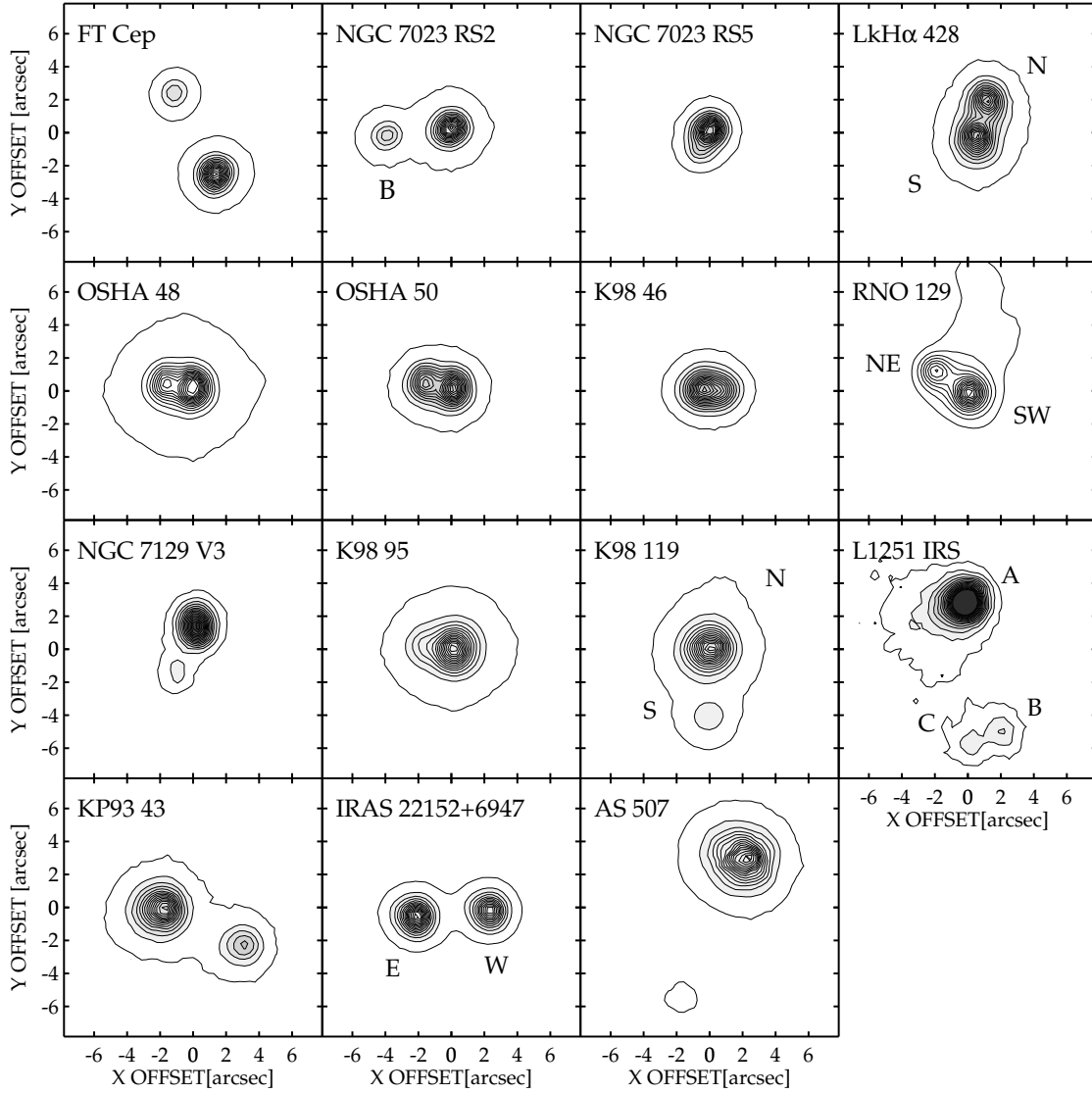


Fig. 5.— Visual double stars of our sample, consisting of components separated by $\sim 1 - 10''$. $15.6'' \times 15.6''$ (51×51 pixels) parts of I_C images are plotted.

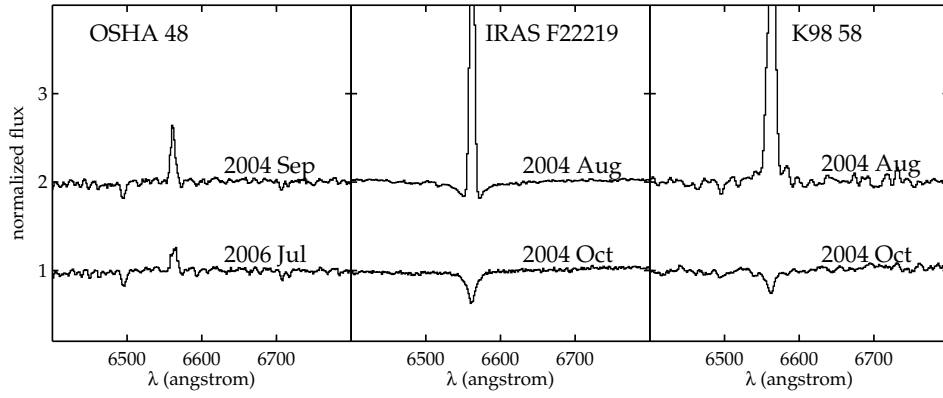


Fig. 6.— Spectra displaying variable H α line.

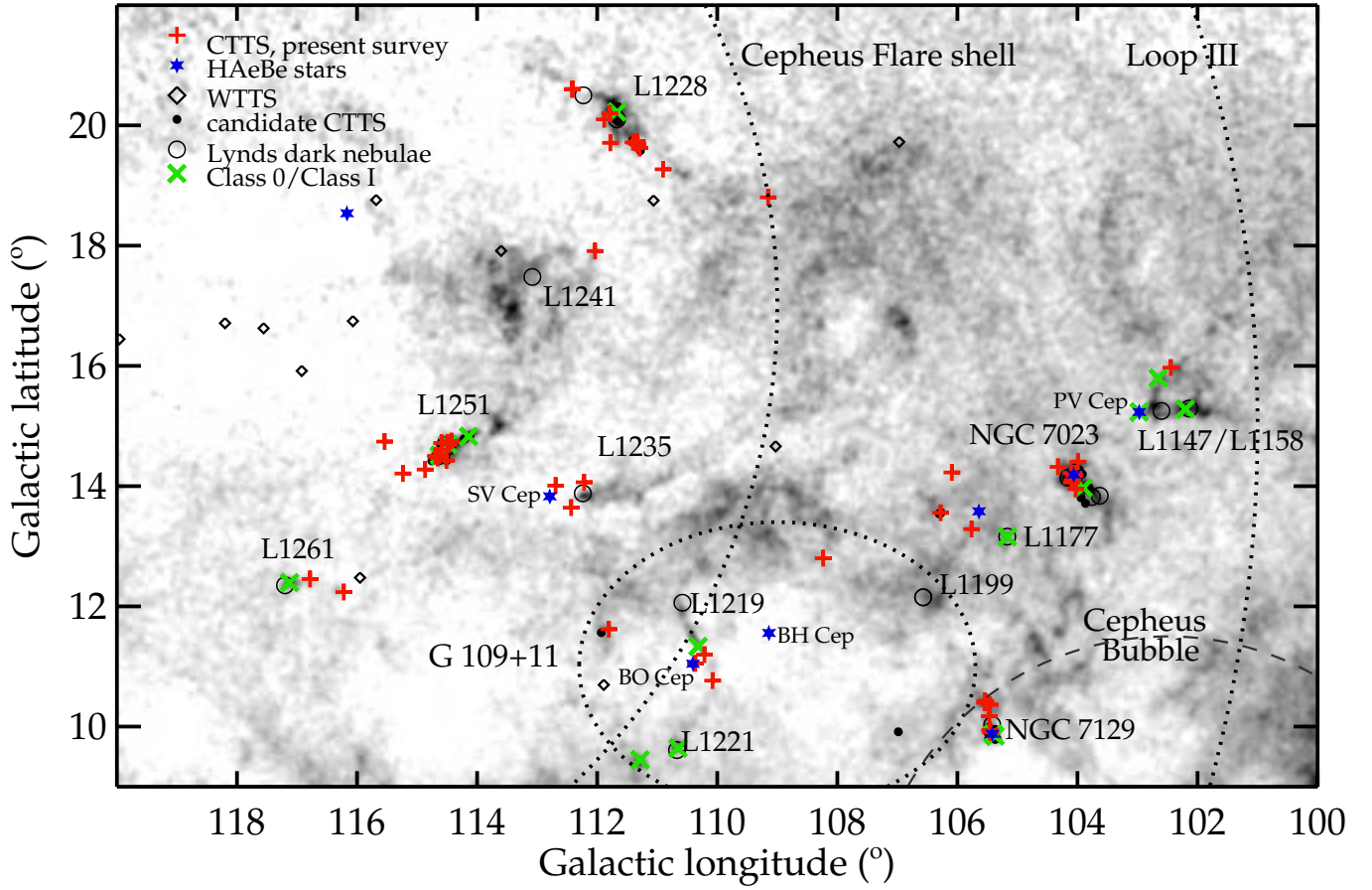


Fig. 7.— Distribution of the PMS stars overlotted on the extinction map of the region (Dobashi et al. 2005). Plusses (red in the electronic version) indicate the CTTSs studied in this paper, and diamonds are WTTs identified by Tachihara et al. (2005). Star symbols show Herbig Ae/Be stars, and black dots are infrared-excess stars based on their near (2MASS) or mid-infrared (Spitzer IRAC) color indices. Crosses (green in the electronic version) show the known Class 0/Class I type objects of the region, indicative of active low-mass star formation. Dotted lines indicate the nearby giant loop structures Loop III, Cepheus flare Shell, and G 109+11, and dashed line shows the more distant Cepheus Bubble.

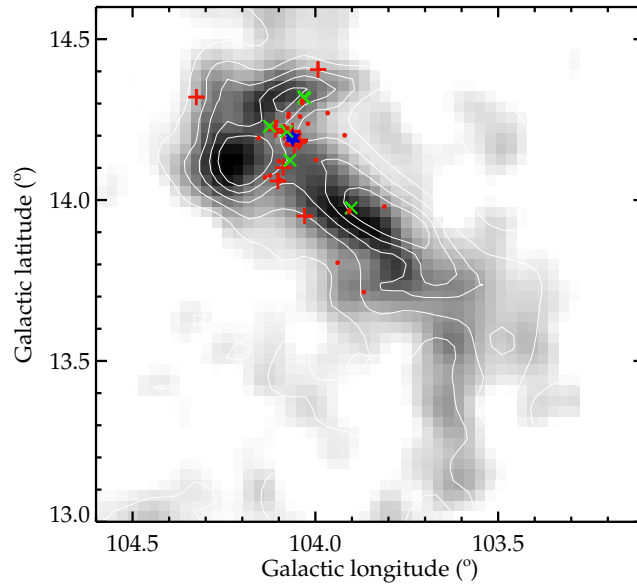


Fig. 8.— Enlarged part of the extinction map shown in Fig. 7, centered on L1174. The lowest contour is at $A_V = 0.7$ mag, and contour interval is 0.5 mag. Plusses (red in the electronic version) show our program stars, crosses (green in the electronic version) are protostellar (Class I) objects. The star symbol (blue in electronic version) indicates HD 200775, the most massive member of NGC 7023. Small dots (red in the electronic version) are Class II YSOs detected by Spitzer (Kirk et al. 2009).

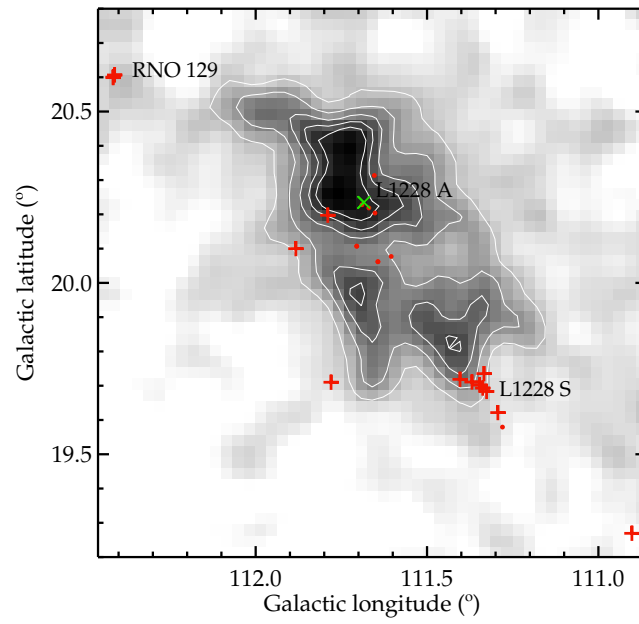


Fig. 9.— Enlarged part of Fig. 7, centered on L 1228. Extinction contours and symbols are same as in Fig. 8.

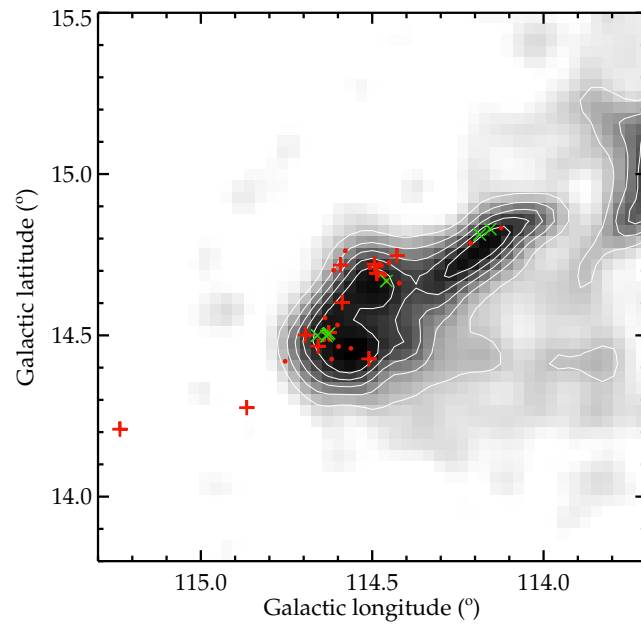


Fig. 10.— Same as Fig. 8, but centered on L 1251. Symbols are same as in Fig. 8.

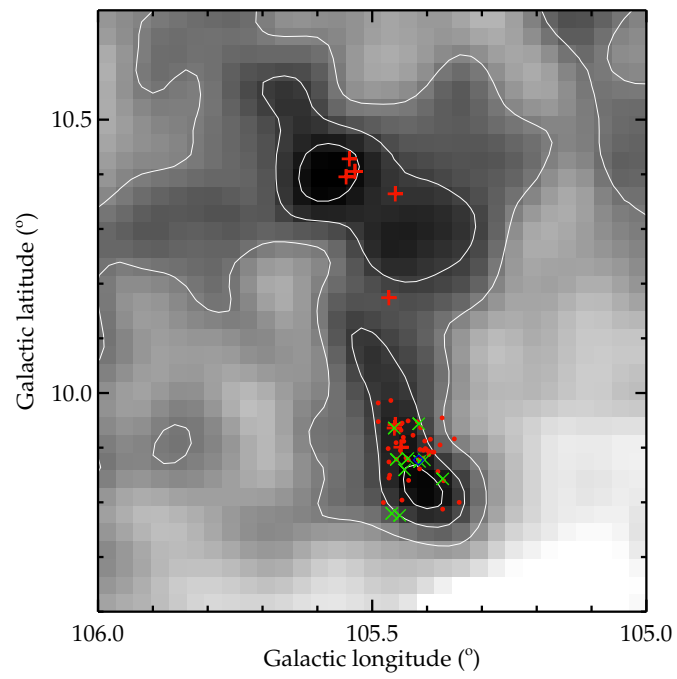


Fig. 11.— Enlarged part of Fig. 7, centered on NGC 7129. Symbols are same as in Fig. 8.

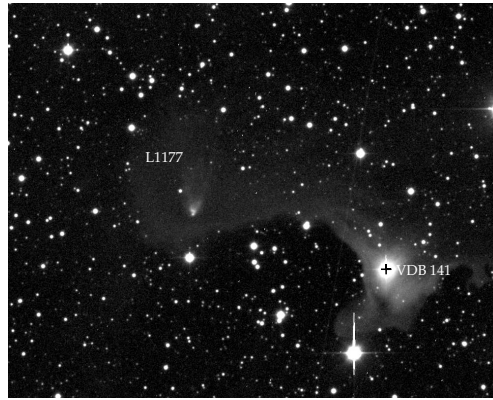


Fig. 12.— An I-band image of a $17' \times 13'.5$ area of the dark cloud L 1177 (CB 230), and the reflection nebula VDB 141, obtained with the Schmidt telescope of the Konkoly Observatory. L 1177 is obviously connected with the cloud illuminated by VDB 141, though the presence of the star within the cloud is accidental.

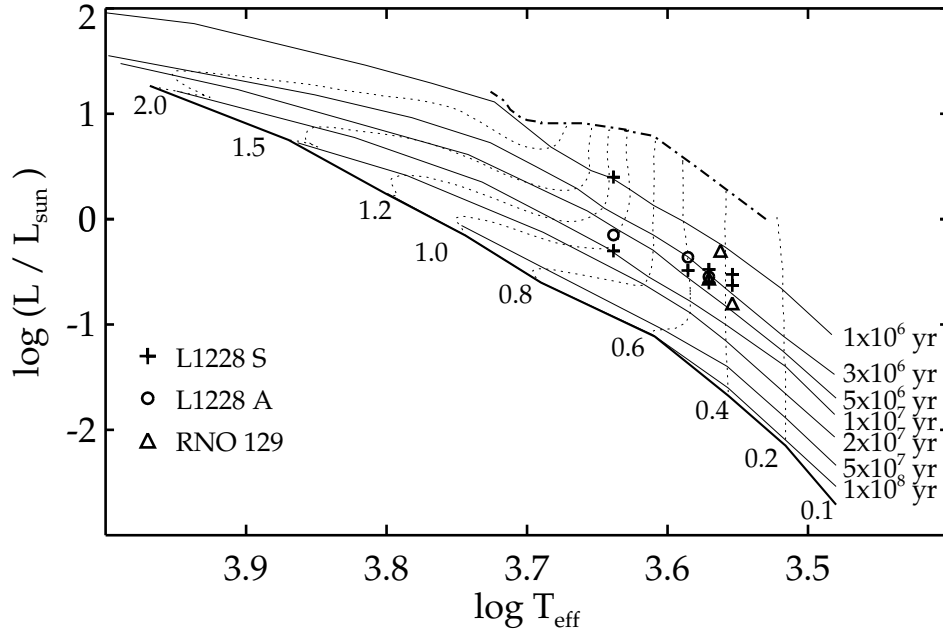


Fig. 13.— Hertzsprung–Russell diagram of the PMS stars of L 1228, assuming a distance of 200 pc. Thin solid lines indicate the isochrones as labelled, and dotted lines show the evolutionary tracks for the masses (in solar masses) indicated at the lower end of the tracks according to Palla & Stahler (1999) model. The dash-dotted line corresponds to the birthline and thick solid line indicates the zero age main sequence (ZAMS). Plusses indicate the members of the aggregate L 1228 S (Padgett et al. 2004), circles are the stars near the core L 1228 A (Bally et al. 1995), and triangles show the three stars embedded in the reflection nebula RNO 129 (Movsessian & Magakian 2004).

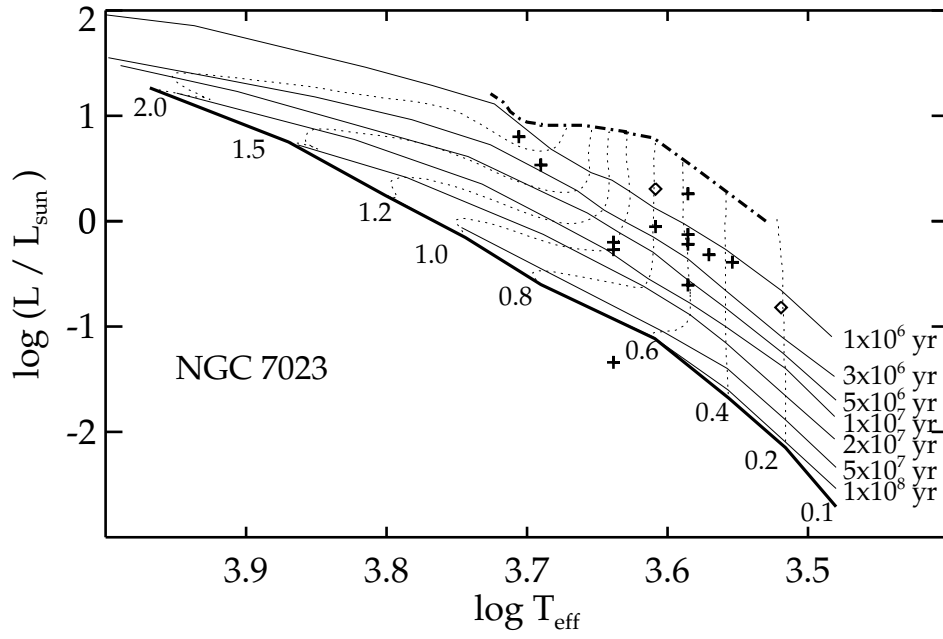


Fig. 14.— Same as Fig. 13, for the PMS stars of NGC 7023, assuming a distance of 330 pc. Diamonds show the positions of both components of the visual binary LkH α 428. The star below the ZAMS is NGC 7023 RS 10.

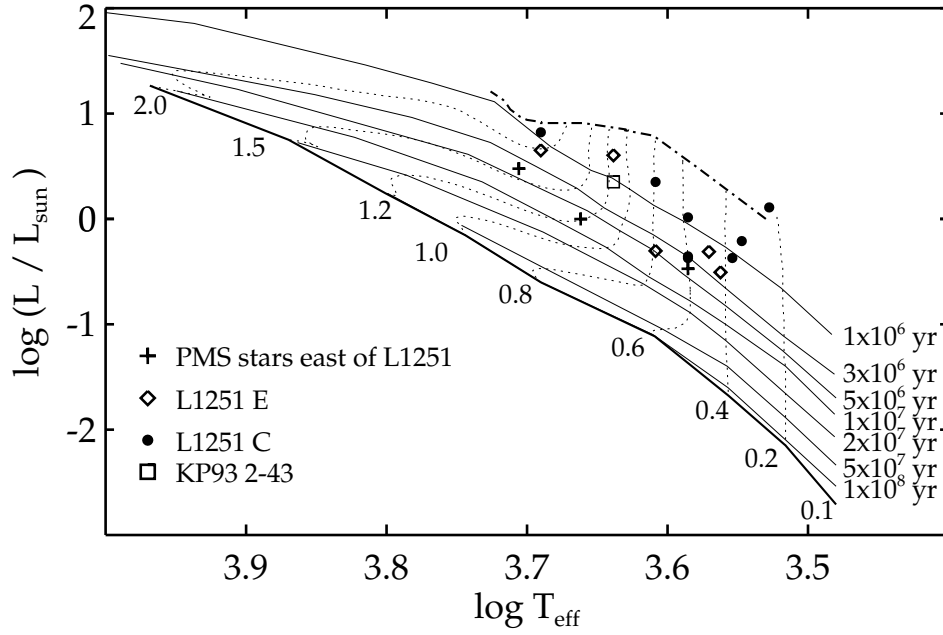


Fig. 15.— Same as Fig. 13, for the PMS stars of L 1251, assuming a distance of 320 pc. Plusses show the three PMS stars on the high-longitude side of the cloud, diamonds are the stars associated with the C^{18}O core L 1251 E (Sato et al. 1994; Lee et al. 2006), and dots are the stars associated with the core L 1251 C (Sato et al. 1994). Open square marks the WTTS [KP93] 2-43. It can be seen that the PMS stars on the high-longitude side of the cloud are older than those projected inside the molecular cloud, indicating that star formation propagates from the higher towards the lower Galactic longitudes.

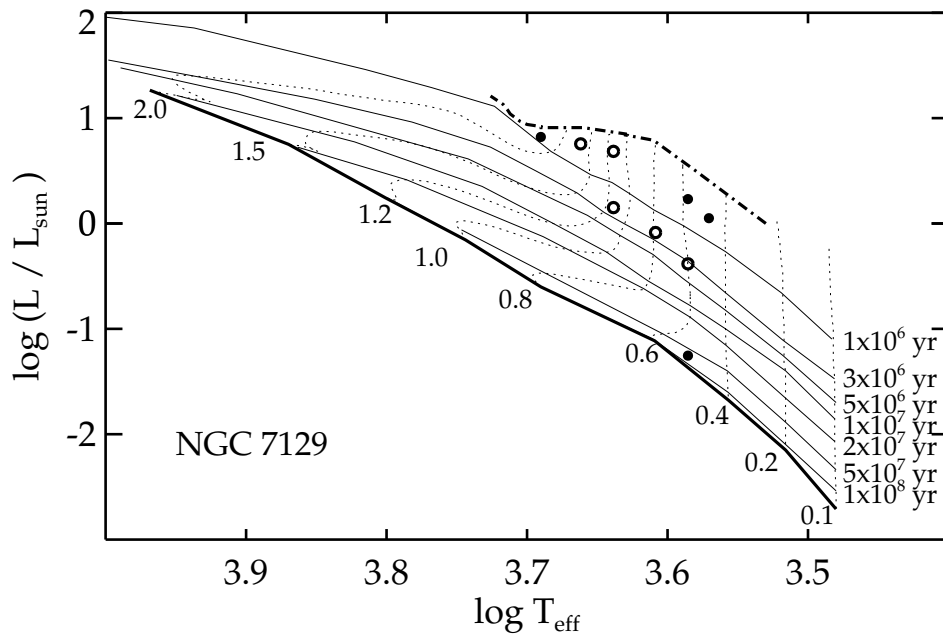


Fig. 16.— Same as Fig. 13, for the PMS stars of NGC 7129, assuming a distance of 800 pc. Filled circles show the stars associated with the central cluster, and open symbols indicate those found in the high-latitude clump of L1181. The stars close to the birthline suggest that NGC 7129 is probably not farther than the adopted distance. The star near the ZAMS is GGD 33a, probably a Class I source.

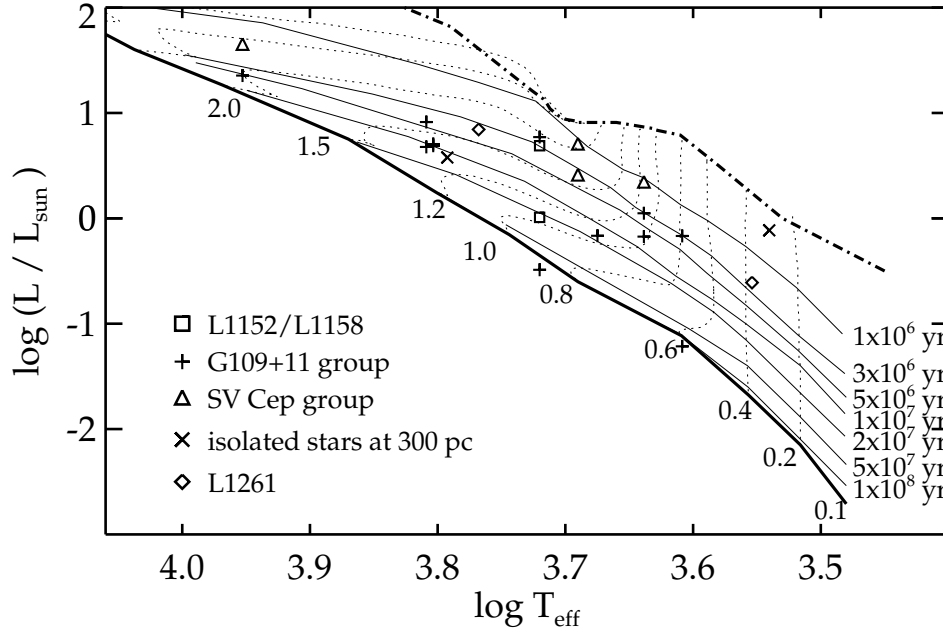


Fig. 17.— HRD of the PMS stars associated with L 1152/L 1158, L 1219, SV Cep, L 1261/L 1262, and the PMS stars dispersed over the Cepheus flare. The stars below the ZAMS are [K98c] Em* 58 and [K98c] Em* 119 S, probably edge-on disk systems. IRAS F22219+7901 is not plotted.

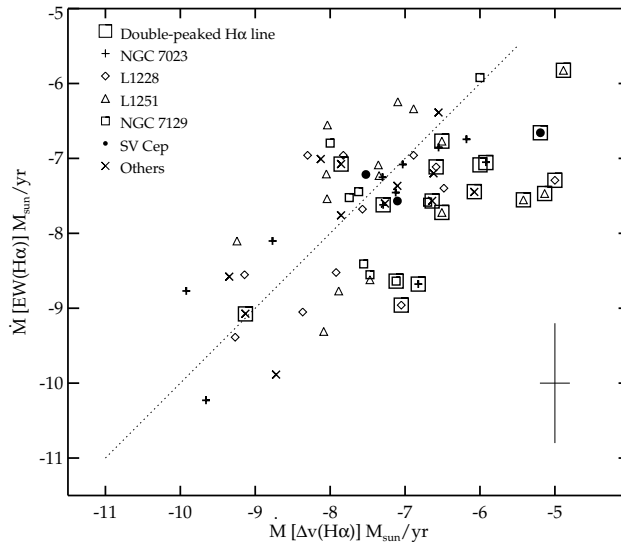


Fig. 18.— Accretion rates derived from the $H\alpha$ luminosities, plotted against those derived from the 10% width of the $H\alpha$ emission line. Different symbols indicate the stars belonging to different clouds. Symbols framed by large squares mark the stars exhibiting double-peaked $H\alpha$ line. The formal estimated error of the points is shown in the lower right corner.

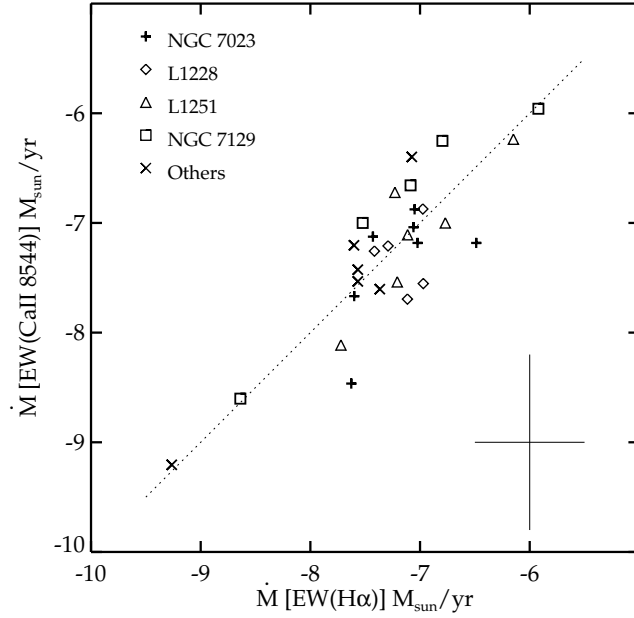


Fig. 19.— Accretion rates derived from the Ca II luminosities, plotted against those derived from the H α luminosities. The errorbar is shown in the lower right corner.

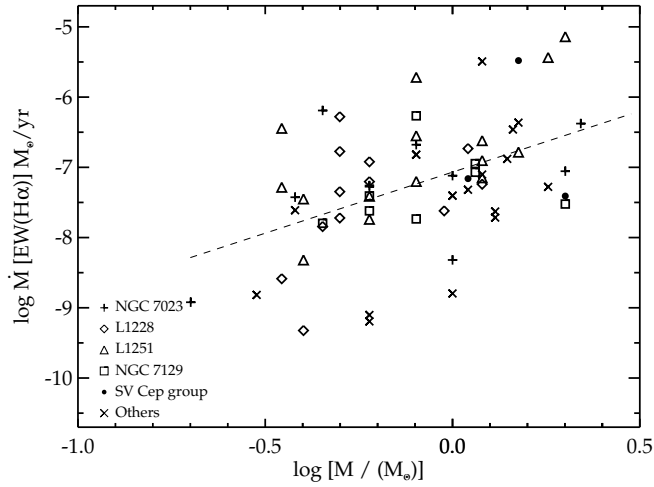


Fig. 20.— Accretion rates derived from the H α lines plotted against the stellar masses determined from the HRD. The dashed line, fitted to the data corresponds to $\log \dot{M} = (1.74 \pm 0.40) \times \log M - 7.07 \pm 0.10$.

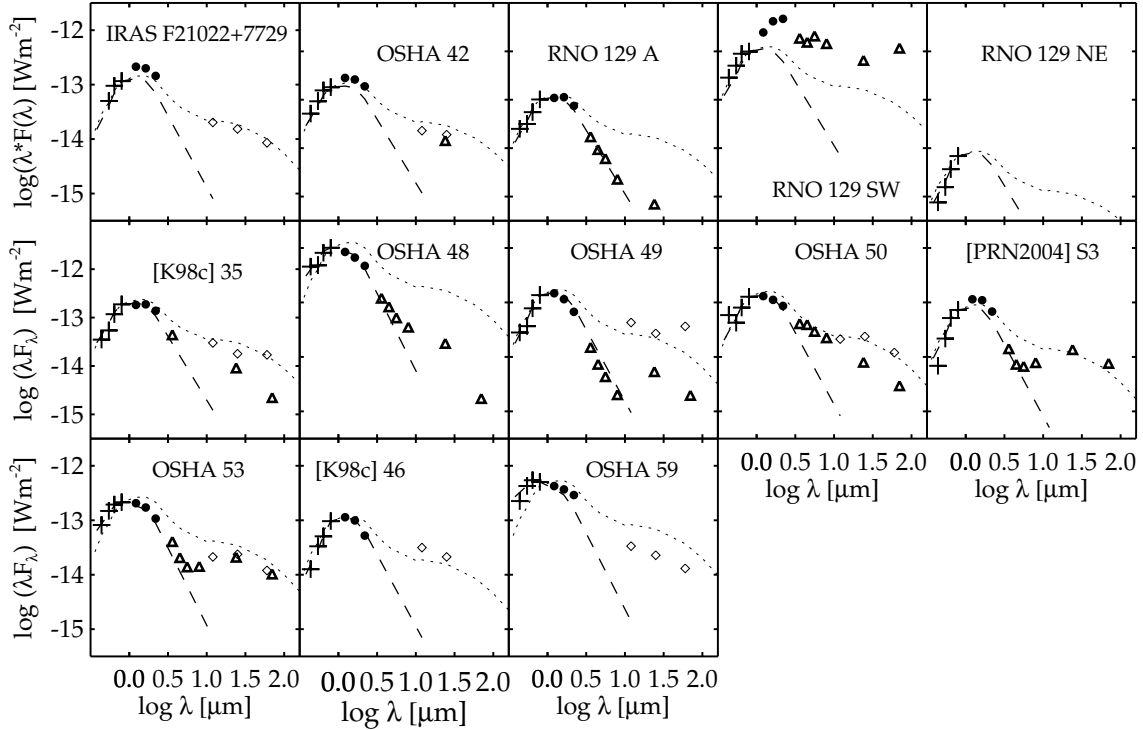


Fig. 21.— Spectral energy distributions, corrected for interstellar extinction, of the PMS stars in the region of L 1228, based on our optical photometry (plusses), 2MASS (dots), *Spitzer* IRAC and MIPS (triangles), as well as *IRAS* (thin diamonds) data. Dashed lines show the photospheric SEDs. Their values were determined from the dereddened I_C magnitudes, and from the colour indices corresponding to the spectral types. For comparison, dotted lines show the median SED of the T Tauri stars of the Taurus star forming region (D’Alessio et al. 1999).

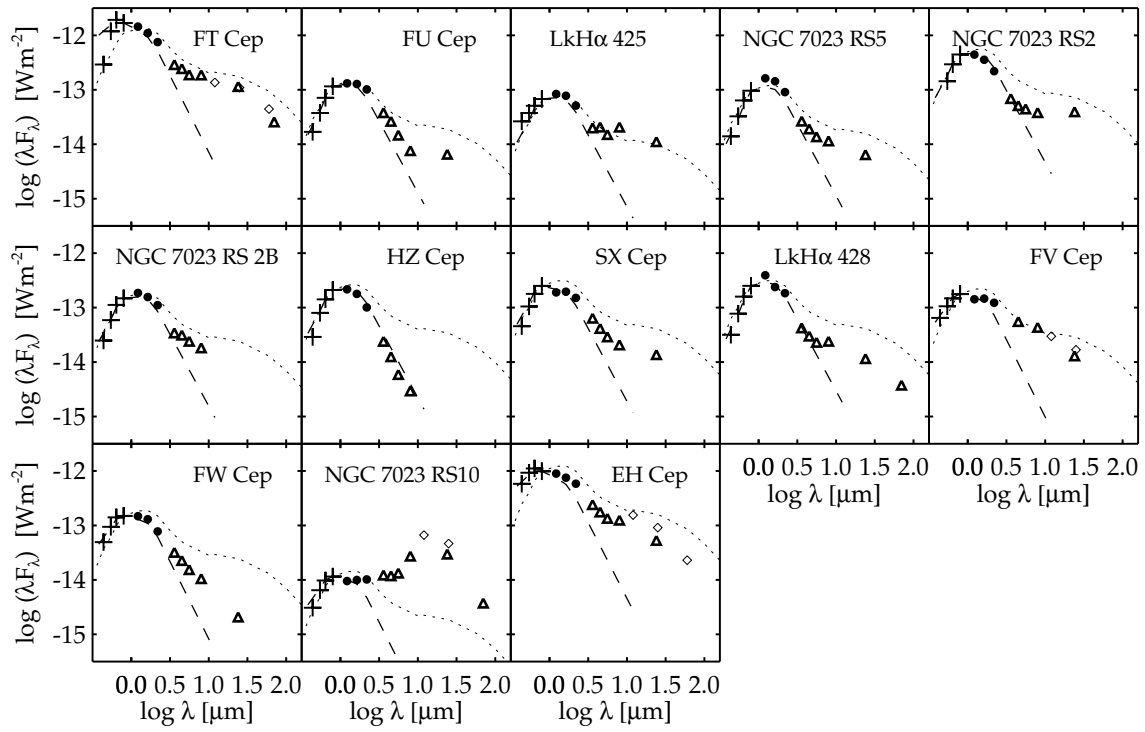


Fig. 22.— Same as Fig. 21, but for the PMS stars of NGC 7023.

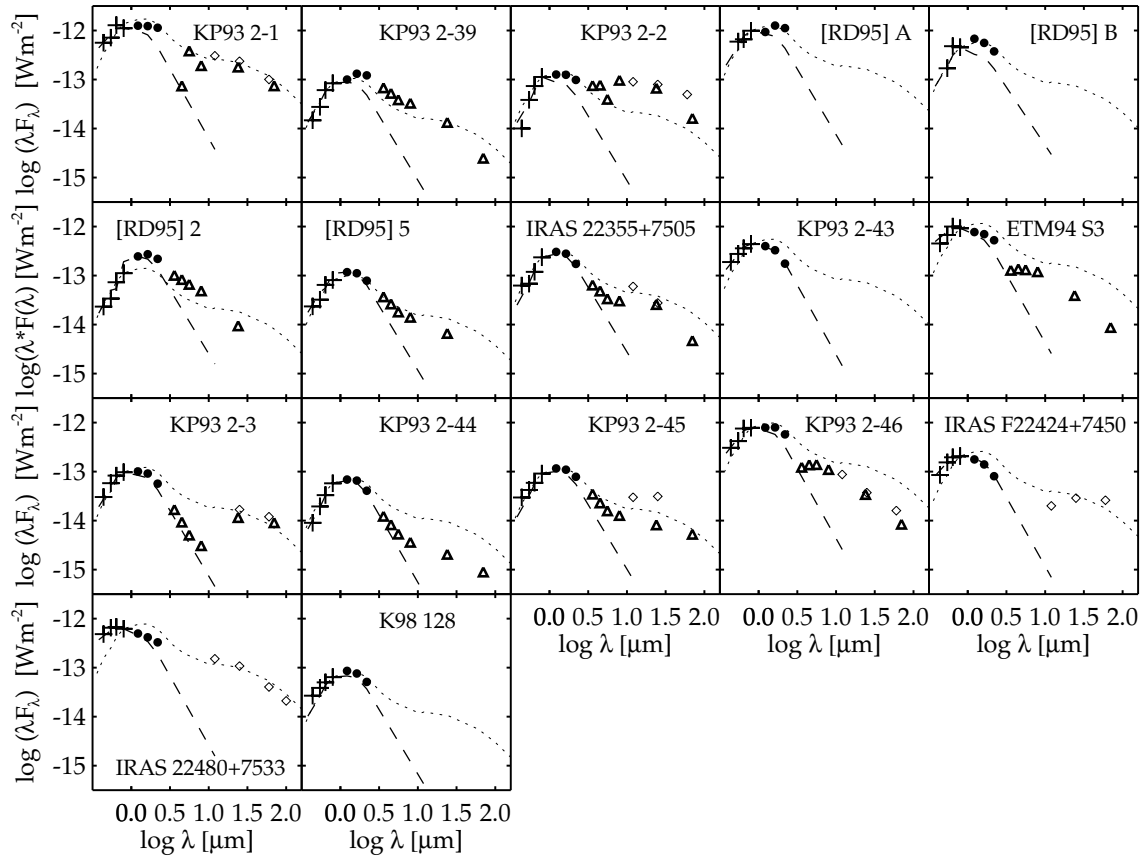


Fig. 23.— Same as Fig. 21, but for the PMS stars of L 1251.

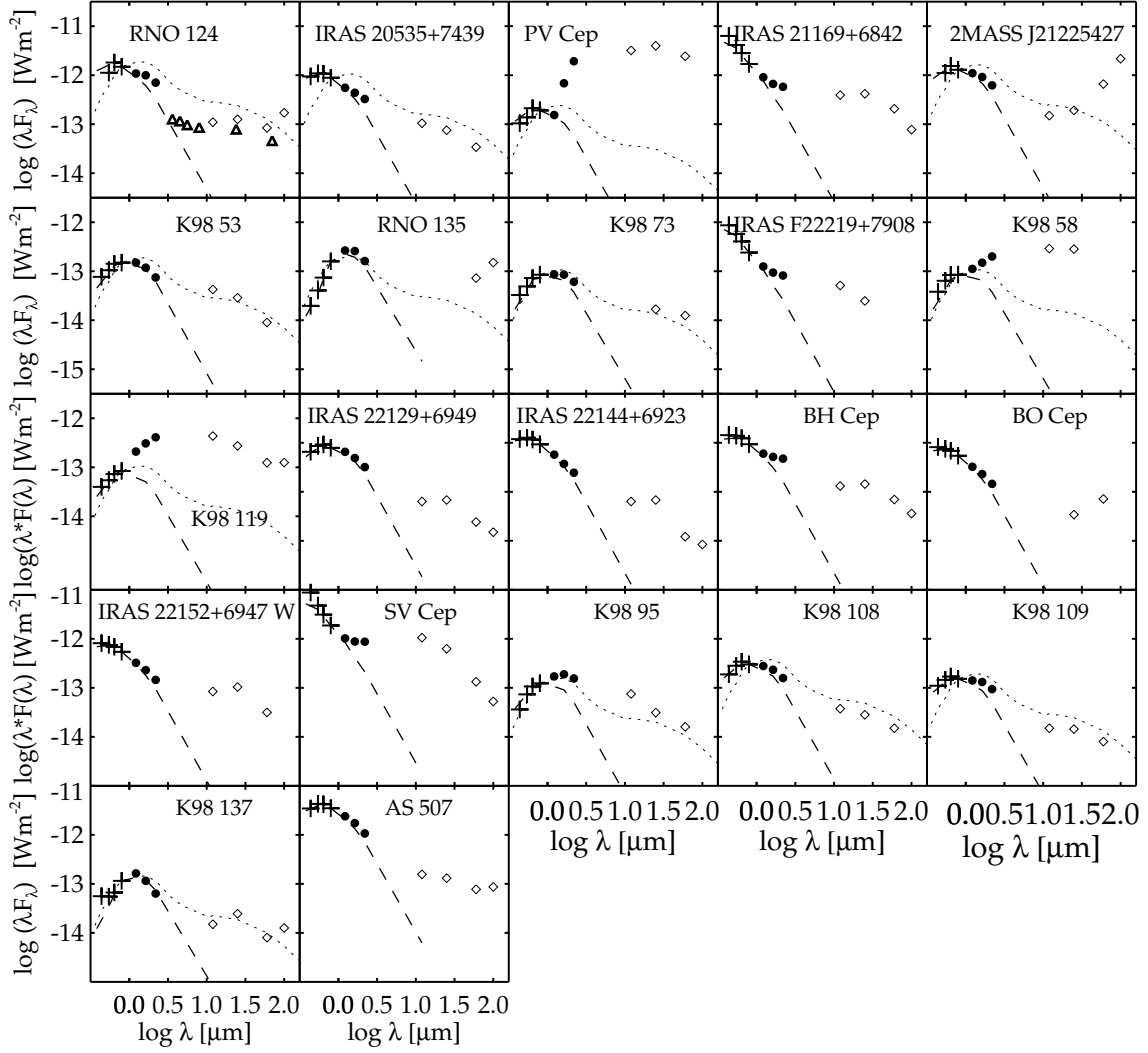


Fig. 24.— Same as Fig. 21, but for the stars associated with L 1152/L 1158, L 1177, L 1219, SV Cep, L 1261/L 1262, and the PMS stars dispersed over the cloudy region.

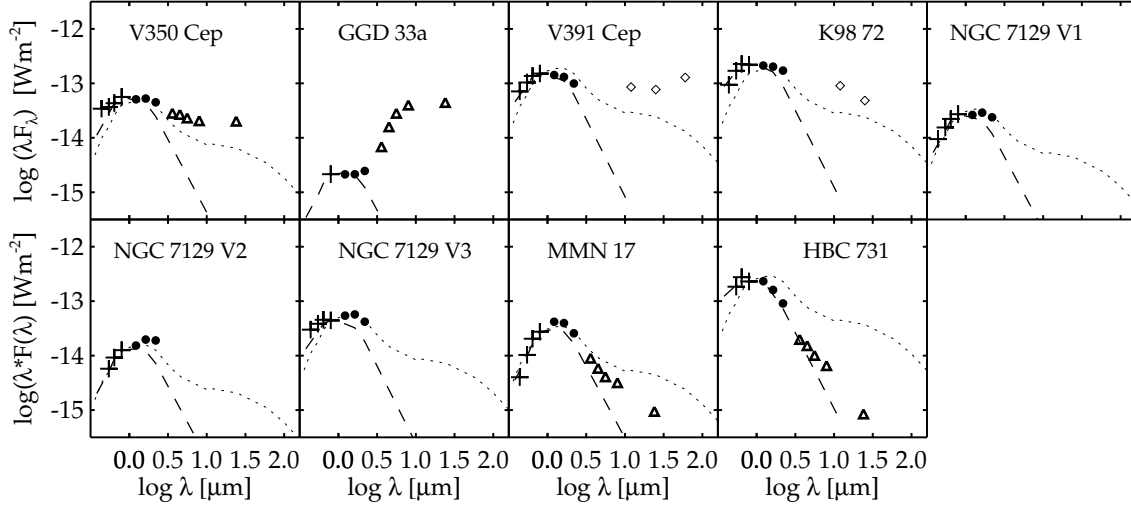


Fig. 25.— Same as Fig. 21, but for the observed PMS stars of NGC 7129.

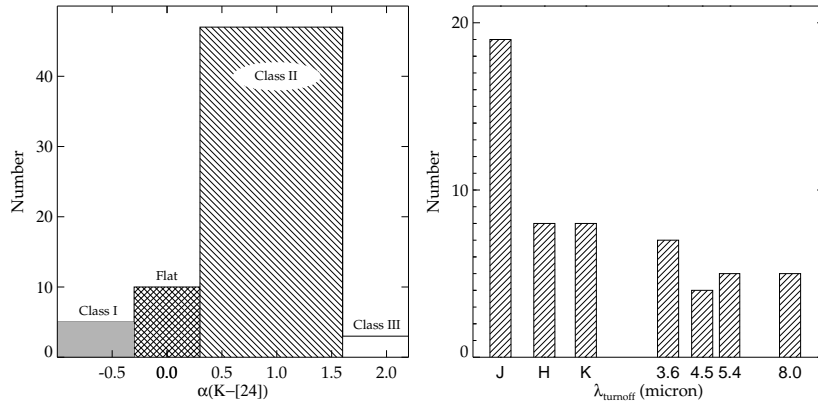


Fig. 26.— *Left*: distribution of the SED classes defined by the slope α_{24-K} ; *Right*: Number of stars whose observed SED has the last photospheric value in the photometric band indicated in the horizontal axis.

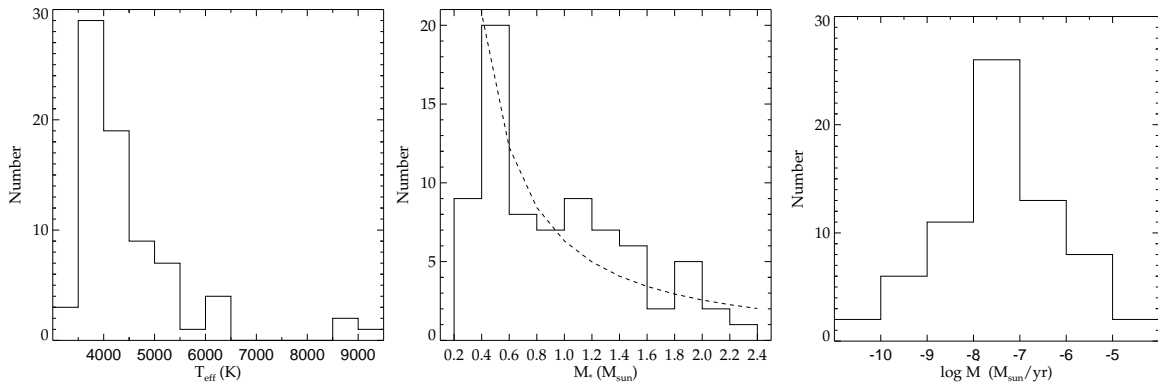


Fig. 27.— Frequency distribution of effective temperatures, masses, and accretion rates. The shape of the Salpeter IMF is indicated by dashed line in the middle panel.

Table 1. List of the observed PMS stars and associated clouds

Names	IRAS	2MASS	Spitzer Id.*	Membership	Cand. Type	Ref.
RNO 124, HBC 695, [K98c] Em* 6	20359+6745	20361986+6756316	3	L 1152	CTTS	3
PV Cep, HBC 696, RNO 125, [K98c] Em* 9	20453+6746	20455394+6757386	135	L 1155	CTTS	3
GSC 04472-00143	20535+7439	20530638+7450348	IRAS	8
OSHA 42, [K98c] Em* 30	F20598+7728	20584668+7740256	123	L 1228	H α	5,8
RNO 129 A		20590373+7823088	...	L 1228	red, nebulous	18
RNO 129 SW, Bern 48, [K98c] Em* 32, OSHA 44	21004+7811	20591409+7823040	...	L 1228	IRAS	5,18
RNO 129 NE ^a	21004+7811	20591409+7823040	...	L 1228	IRAS	5,18
FT Cep, NGC 7023 RS 1, [K98c] Em* 26	20587+6802	20592284+6814437	15	NGC 7023	variable, H α	3
[K98c] Em* 35, [PRN2004] S5	F21016+7651	21005285+7703149	124	L 1228	H α , MIR	8,12
...	F21022+7729	21011339+7741091	...	L 1228	IRAS	8
NGC 7023 RS 2, NGC 7023 S J		21012637+6810385	27	NGC 7023	variable	1,4
NGC 7023 RS 2 B ^b		21012706+6810381	137	NGC 7023	variable	1
OSHA 48 A, [PRN2004] S6		21012919+7702373	30	L 1228	H α	5,12
OSHA 48 B		21012919+7702373	...	L 1228	H α	5,12
OSHA 49, [K98c] Em* 40, [PRN2004] S7	F21023+7650	21013097+7701536	32	L 1228	H α	5,8,12
OSHA 50, [K98c] Em* 41, [PRN2004] S8		21013267+7701176	33	L 1228	H α	5,8,12
PW Cep, LkH α 425, NGC 7023 RS 3, NGC 7023 S E		21013590+6808219	104	NGC 7023	variable, H α	1,4
SX Cep, NGC 7023 S L		21013754+6811309	...	NGC 7023	variable	1,4
NGC 7023 RS 5, NGC 7023 S N		21014250+6812572	38	NGC 7023	variable	1,4
HZ Cep, RS S3, NGC 7023 S D		21014358+6809361	...	NGC 7023	variable	1,4
FU Cep, LkH α 427, HBC 304, NGC 7023 S C	21009+6758	21014672+6808453	...	NGC 7023	CTTS	2,4
[PRN2004] S3		21014960+7705479	42	L 1228	MIR excess	12
OSHA 53, [K98c] Em* 43, [PRN2004] S9	F21028+7645	21020488+7657184	43	L 1228	H α	5,8,12
FV Cep, LkH α 275, HBC 306, [K98c] Em* 38	F21017+6813	21022039+6825240	46	NGC 7023	CTTS	3
LkH α 428 N, NGC 7023 RS 8		21022829+6803285	125	NGC 7023	H α	1
LkH α 428 S ^b		21022829+6803285	52	NGC 7023	H α	1
FW Cep, NGC 7023 RS 9		21023299+6807290	55	NGC 7023	variable	1
NGC 7023 RS 10	21023+6754	21025943+6806322	57	NGC 7023	variable, IRAS	1
[K98c] Em* 46	F21037+7614	21030242+7626538	...	L 1228	H α , IRAS	8
EH Cep, LkH α 276, HBC 307, [K98c] Em* 42	21027+6747	21032435+6759066	60	NGC 7023	CTTS	3
OSHA 59, [K98c] Em* 49	F21066+7710	21055189+7722189	...	L 1228	H α	5,8
[K98c] Em* 53		21153595+6940477	H α	8
BD +68° 1118, GSC 04461-01336	21169+6842	21173917+6855097	...	L 1177?	IRAS	8
[K98c] Em* 58	F21202+6835	21205785+6848183	H α , IRAS	8
2MASS 21225427+6921345		21225427+6921345	K-band excess	17

Table 1—Continued

Names	IRAS	2MASS	Spitzer Id.*	Membership	Cand. Type	Ref.
RNO 135, [K98c] Em* 61	21326+7608	21323108+7621567	...	L 1241?	H α , IRAS	8
NGC 7129 S V1		21401174+6630198	...	NGC 7129	variable	9
NGC 7129 S V2		21402277+6636312	...	NGC 7129	variable	9
V391 Cep, [K98c] Em* 71	F21394+6621	21402755+6635214	...	NGC 7129	CTTS	8,19
NGC 7129 S V3		21403852+6635017	...	NGC 7129	variable	9
[K98c] Em* 72	F21404+6608	21413315+6622204	...	NGC 7129	H α	8
HBC 731, [SVS76] NGC 7129 6		21425961+6604338	NGC 7129 30	NGC 7129	CTTS	2,3
HBC 732, V350 Cep, [MMN2004b] 13		21430000+6611279	NGC 7129 31	NGC 7129	CTTS	3,10,11
GGD 33A		21430320+6611150	NGC 7129 5	NGC 7129	HH, H α	10
[MMN2004b] 17		21431161+6609114	NGC 7129 43	NGC 7129	H α	11
[K98c] Em* 73		21443229+7008130	H α	8
BH Cep, HBC 734, [K98c] Em* 83	22006+6930	22014287+6944364	...	L 1219?	HAeBe	3
[K98c] Em* 95		22131219+7332585	...	L 1235?	H α	8
GSC 04467-00835	22129+6949	22140608+7005043	...	L 1219	IRAS	8
TYC2 4467-324-1	22144+6923	22154189+6938566	...	L 1219	IRAS	8
TYC 4467-836-1	22152+6947	22163111+7002393	...	L 1219	IRAS	8
BO Cep, HBC 735, [K98c] Em* 100	F22156+6948	22165406+7003450	...	L 1219?	HAeBe	3
[K98c] Em* 109		22190169+7346072	...	L 1235?	H α	8
[K98c] Em* 108		22190203+7319252	...	L 1235?	H α	8
SV Cep, HBC 736, [K98c] Em* 113	22205+7325	22213319+7340270	HAeBe	3
TYC 4608-2063-1	22219+7908	22220233+7923279	IRAS	8
[K98c] Em* 119 N	22256+7102	22265660+7118011	H α	8
[K98c] Em* 119 S	22256+7102	22265660+7118011	H α	8
[KP93] 2-1, XMMU J223412.2 +751809	22331+7502	22341189+7518101	142	L 1251	H α	6,13
[KP93] 39, XMMU J223516.6 +751848		22351668+7518471	76	L 1251	H α	6,13
[RD95] B, VLA 10?	22343+7501	22352442+7517037	143?	L 1251	IR, radio?	14,15,16
[RD95] A, VLA 7, VLA B	22343+7501	22352497+7517113	143?	L 1251	IR, radio	14,15,16
[RD95] 2		22352542+7517562	77	L 1251	K-band excess	16
[RD95] 5		22352722+7518019	79	L 1251	K-band excess	16
[KP93] 2-2, XMMU J223605.8 +751831	22350+7502	22360559+7518325	80	L 1251	H α	6,13
[KP93] 3-10	22355+7505	22363545+7521352	81	L 1251	IRAS	6
[KP93] 2-43, XMMU J223727.7 +751525		22372780+7515256		L 1251	H α	6,13
[KP93] 2-3, XMMU J223750.1 +750408		22374953+7504065	83	L 1251	H α	6,13
[ETM94] IRAS 22376+7455 Star 3, XMMU J223818.8 +751154		22381872+7511538	86	L 1251	H α	6,10

Table 1—Continued

Names	IRAS	2MASS	Spitzer Id.*	Membership	Cand. Type	Ref.
[KP93] 2-44, [ETM94]IRAS 22376+7456 Star 1, XMMU J223842.5+751146		22384249+7511455	107	L 1251	H α	6,7,13
[KP93] 2-45, XMMU J223927.3 +751029		22392717+7510284	96	L 1251	H α	6,13
[KP93] 2-46, XMMU J223942.9 +750644	22385+7457	22394030+7513216	97	L 1251	H α	6,13
GSC 04601-03483	F22424+7450	22433926+7506302	...	L 1251	IRAS	8
[K98c] Em* 128		22490470+7513145	...	L 1251	H α	8
TYC 4601-1543-1	22480+7533	22491626+7549438	...	L 1251	IRAS	8
[K98c] Em* 137		23143398+7350022	...	L 1261	H α	8
AS 507, HBC 741, V395 Cep, [K98c] Em* 140	23189+7357	23205208+7414071	...	L 1261	CTTS	3

References. — (1) Rosino & Romano (1962); (2) Strom et al. (1976); (3) Herbig & Bell (1988); (4) Sellgren (1983); (5) Ogura & Sato (1990); (6) Kun & Prusti (1993); (7) Eiroa et al. (1994); (8) Kun (1998); (9) Semkov (2003); (10) Miranda et al. (1994); (11) Magakian et al. (2004); (12) Padgett et al. (2004); (13) Simon (2006); (14) Beltrán et al. (2001); (15) Meehan et al. (1998); (16) Rosvick & Davidge (1995); (17) Cutri et al. (2003); (18) Movsessian & Magakian (2004); (19) Semkov (1993).

*This column shows the identifier of the stars observed by Spitzer in Gutermuth et al. (2009) (NGC 7129), and in Kirk et al. (2009) (other stars).

^aBinarity of the star embedded in RNO 129 was reported by Magakian et al. (2004). Our observations have shown that both components are PMS stars.

^bBinarity of NGC 7023 RS2 and LkH α 428 was reported by Rosino & Romano (1962). Our observations have shown that both components of these doubles are PMS stars.

Table 2. List of the observed stars rejected as PMS stars

Name	2MASS	Instrument	Comment	Ref.
[K98c] Em* 2	20200929+7351431	CAFOS+R100	dMe	
[K98c] Em* 3	20220638+7301104	CAFOS+R100	dMe	
[K98c] Em* 4	20233729+6807137	CAFOS+R100	planetary nebula	
[K98c] Em* 7	20422058+7229495	FAST	no H α emission	
F20432+7457, 4C 74.26	20423730+7508024	CAFOS+R100	quasar	1
OSHA 1	20433097+7903247	CAFOS+R100	no H α emission	
OSHA 2	20441641+7659130	CAFOS+R100	no H α emission	
OSHA 3	20445359+7542255	CAFOS+R100	no H α emission	

Note. — Table 2 is published in its entirety in the electronic edition of the *Astrophysical Journal*. A portion is shown here for guidance regarding its form and content.

References. — (1) Veron-Cetty, & Veron (2006)

Table 3. Summary of spectroscopic observations^a

Id.	Instrument	Sp.T.	H α shape ^a	Other emission lines
RNO 124	CAFOS+R100	K0	I	[O I] 6300, 6363, He I 5875, 6678, O I 7773, 8446, Ca II triplet, Pa 11,12,14
PV Cep	CAFOS+R100	cont.	IIIB	[O I] 6300, 6363, Fe II 6456, 6516, He I 5875, 6678, [S II] 6716, 6731, [Fe II] 7155 K I 7664, 7698, O I 7773, 8446, Ca II triplet, Pa 11,12,13,14,19
IRAS 20535+7439	CAFOS+R100, FAST	F8	IVR	
OSHA 42	CAFOS+R100	M0	I	[O I] 6300, 6363, He I 6678, [S II] 6716, 6731 O I 7773, 8446, Ca II triplet
RNO 129 A	CAFOS+R100	M1	I	[O I] 6300, 6363
RNO 129 SW	CAFOS+R100, FAST	M1.5	IIIB	[O I] 6300, 6363, [S II] 6716, 6731 [Fe II] 7155, Ca II triplet
RNO 129 NE	CAFOS+R100, FAST	M2	IIIB	Ca II H&K, Balmer ser., Fe II 4351, Fe I 4922, 5016 [O I] 6300, 6363, [S II] 6716, 6731, [Fe II] 7155 [O I] 6300, O I 7773, 8446, Ca II triplet
FT Cep	CAFOS+R100	K1	I	
[K98c] Em* 35	CAFOS+R100	M2	I	
F21022+7729	CAFOS+R100	M1	IIB	[O I] 6300, O I 7773, 8446, Ca II triplet, Pa 11,12,14,19
NGC 7023 RS 2	CAFOS+R100	M0IV	IIB	[O I] 6300
NGC 7023 RS 2 B	CAFOS+R100	M0	I	
OSHA 48	CAFOS+R100, FAST	K5	I	
OSHA 48 B	CAFOS+R100	cont.	I	
OSHA 49	CAFOS+R100, FAST	M1	I	
OSHA 50	CAFOS+R100, FAST	M0	I	Ca II H&K, Balmer ser., Fe I 4922, 5016, [O I] 6300 6363, He I 5875, 6678, Ca II triplet
LkH α 425	CAFOS+R100	M0	I	[O I] 6300, 6363, He I 6678, [S II] 6716, 6731, O I 8446 Ca II triplet
SX Cep	CAFOS+R100	K7	abs.	
NGC 7023 RS 5	CAFOS+R100	M2	I	[O I] 6363, O I 8446, Ca II triplet
HZ Cep	CAFOS+R100	M0	I	
FU Cep	CAFOS+R100	M1	IIIB	He I 6678, O I 8446, Ca II triplet
[PRN2004] S3	CAFOS+R100	M1	I	
OSHA 53	CAFOS+R100, FAST	K5	I	H β
FV Cep	CAFOS+R100	K5	I	He I 6678
LkH α 428 N	CAFOS+R100	K7	I	O I 8446, Ca II triplet
LkH α 428 S	CAFOS+R100	M4.5IV	I	
FW Cep	CAFOS+R100	K5	I	
NGC 7023 RS 10	CAFOS+R100	K4	I	
[K98c] Em* 46	CAFOS+R100	M2	I	

Table 3—Continued

Id.	Instrument	Sp.T.	H α shape ^a	Other emission lines
EH Cep	CAFOS+R100	K2	I	Ca II triplet
OSHA 59	CAFOS+R100, FAST	K5	I	
[K98c] Em* 53	CAFOS+R100, FAST	K5	I	Ca II H&K, Balmer ser., He I 5875, 6678, O I 7773, 8446, Ca II triplet
BD +68° 1118	FAST	A2	I	
[K98c] Em* 58	CAFOS+R100, FAST	K7	IIIB	[O I] 6300, 6363, [S II] 6716, 6731, Ca II triplet
2MASS 21225427+6921345	CAFOS+R100	K3	I	[S II] 6717
RNO 135	CAFOS+R100	M3IV	I	
NGC 7129 S V1	CAFOS+R100	K7	I	He I 6678
NGC 7129 S V2	CAFOS+R100	M0	IIB	
V391 Cep, [K98c] Em* 71	CAFOS+R100	K5	IVB	[O I] 6300, O I 7773, 8446, 6431, Fe II 6456, He I 6678 Ca II triplet, Fe I 8387, 8514, Pa 11,12,14,19
NGC 7129 S V3	CAFOS+R100	K5	I	
[K98c] Em* 72	CAFOS+R100	K4	IIIB	[O I] 6300, O I 7773, 8446, Ca II triplet
HBC 731	CAFOS+G100	K2	I	
V350 Cep	CAFOS+R100	M0	I	[O I] 6300, He I 6678, [S II] 6716, 6731, Fe II 7711 O I 7773, 8446, Fe I 8327, Ca II triplet
GGD 33A	CAFOS+R100	M0	IIB	[O I] 6300, 6363, [S II] 6716, 6731, Fe I 7282, O I 8446, Ca II triplet
[MMN2004b] 17	CAFOS+R100	M1	I	
[K98c] Em* 73	CAFOS+R100	K7	I	He I 6678, O I 8446, Ca II triplet
BH Cep	CAFOS+G100	F5	IIB	
[K98c] Em* 95	CAFOS+R100, FAST	K5	IIB	O I 7773, 8446, Ca II triplet
IRAS 22129+6949	CAFOS+G100, FAST	K0	I	
IRAS 22144+6923	CAFOS+R100	F6	IIR	O I 8446, Ca II triplet
IRAS 22152+6947W	CAFOS+G100, FAST	F5	abs.	
BO Cep	CAFOS+G100	F5	IIR	
[K98c] Em* 109	CAFOS+R100, FAST	K2	IIR	Balmer ser., He I 5875, 6678, [O I] 6300, [S II] 6731, O I 7773, 8446, Ca II triplet
[K98c] Em* 108	CAFOS+R100, FAST	K2	I	
SV Cep	CAFOS+G100	A2	I	
IRAS F22219+7908	CAFOS+R100, FAST	A1	I	O I 7773, 8446, Ca II triplet
[K98c] Em* 119 N	CAFOS+R100, FAST	K5	I	He I 6678, O I 8446, [S II] 6731, Ca II triplet
[K98c] Em* 119 S	CAFOS+R100, FAST	K0	I	Ca II H&K, H β , Fe I 4922, Na I D, [O I] 6300, O I 8446 He I 5875, 6678, 7065, [S II] 6716, 6731, [Fe II] 7155
[KP93] 2-1	CAFOS+G100	K2	IIB	H β , Fe II 4923, [O I] 6300, 6364, He I 5875, 6678, [S II] 6717, 6731
[KP93] 2-39	CAFOS+G100	M0	I	
[RD95] B	CAFOS+R100	M0	I	[O I] 6300, Ca II triplet

Table 3—Continued

Id.	Instrument	Sp.T.	H α shape ^a	Other emission lines
[RD95] A	CAFOS+R100	K7	I	[O I] 6300, 6363, Ca II triplet
[RD95] 2	CAFOS+R100	M2.5IV	I	Ca II triplet
[RD95] 5	CAFOS+R100	M0IV	I	[O I] 6300
[KP93] 2-2	CAFOS+R100	M2	I	[O I] 6300, He I 6678, [S II] 6716, 6731, O I 7773, 8446
IRAS 22355+7505	CAFOS+G200	M4	I	
[KP93] 2-43	FAST	K5	I	
[KP93] 2-3	CAFOS+G100	K7	I	
[ETM94] Star 3	CAFOS+R100	K2	IIB	O I 8446, Ca II triplet
[KP93] 2-44	CAFOS+G100	M1.5	I	H β , [O I] 6300, 6363, [NII] 6584, [S II] 6716, 6731
[KP93] 2-45	CAFOS+G100	M1	I	H β , He I 5875, 6678
[KP93] 2-46	CAFOS+G100	K5	I	
IRAS F22424+7450	CAFOS+R100, FAST	K4	I	
[K98c] Em* 128	CAFOS+R100	M0	IIIB	He I 6678, O I 7773, Ca II triplet, Pa 11,12,14
IRAS 22480+7533	CAFOS+R100	K1	IIB	O I 7773, 8446, Ca II triplet
[K98c] Em* 137	CAFOS+R100	M2	I	He I 6678
AS 507	CAFOS+G100	G2	I	

^aThe type of the H α emission line is indicated using the scheme introduced by Reipurth, Pedrosa & Lago (1996), i.e. type I lines are symmetric, IIR and IIB are double-peaked with a secondary peak higher than half of the primary located on its red and the blue side, respectively. Type III lines are double-peaked with a secondary peak lower than half of the primary, and IVB and IVR denotes the P Cygni and reversed P Cygni type profiles, respectively.

Table 4. Spectral characteristics of the observed stars

Id.	H α line		EW(CaII triplet)			EW(LiI)	PMS Class
	EW (\AA)	$\Delta v(10\%)$ (km s^{-1})	8499 (\AA)	8545 (\AA)	8663 (\AA)	(\AA)	
RNO 124	-52.2	615	-9.3	-8.7	-8.3	0.30	CTTS
PV Cep	-71.2	481	-76.5	-71.6	-68.0	...	CTTS
IRAS 20535+7439	-3.8	399	0.32	CTTS
OSHA 42	-82.3	516	-4.9	-2.9	-2.3	...	CTTS
RNO 129 A	-6.0	430	WTTS
RNO 129 SW	-36.8	658	-8.4	-8.3	-4.6	...	CTTS
RNO 129 NE	-5.0	622	-1.2	-0.8	-0.8	...	CTTS
FT Cep	-9.6	573	-2.8	-2.1	-2.2	0.36	CTTS
[K98c] Em* 35	-7.4	426	0.48	CTTS
F21022+7729	-91.0	793	-10.8	-13.3	-12.9	...	CTTS
NGC 7023 RS 2	-59.8	543	-0.6	-0.6	-0.9	...	CTTS
NGC 7023 RS 2 B	-63.9	488	CTTS
OSHA 48	-12.6, -2.3	399	0.48	CTTS
OSHA 48 B	-79.6	551	CTTS
OSHA 49	-7.3	283	0.60	CTTS
OSHA 50	-65.0, -78.8	487	-11.0	-11.0	-10.8	...	CTTS
LkH α 425	-106.0	563	-21.5	-22.3	-18.5	...	CTTS
SX Cep	2.15	...	+1.2	+2.3	+0.9	0.61	WTTS
NGC 7023 RS 5	-28.8	544	0.50	CTTS
HZ Cep	-3.9	239	0.46	WTTS
FU Cep	-64.5	691	-3.5	-3.4	-3.1	...	CTTS
[PRN2004] S3	-9.0	526	CTTS
OSHA 53	-20.5, -28.4	515	CTTS
FV Cep	-11.5	378	0.55	CTTS
LkH α 428 N	-56.0	624	-2.1	-2.6	-1.4	0.63	CTTS
LkH α 428 S	-7.5	361	0.50	CTTS
FW Cep	-4.0	596	0.56	CTTS
NGC 7023 RS 10	-8.1	272	+0.5	+1.6	+1.0	...	CTTS
[K98c] Em* 46	-5.3	321	CTTS
EH Cep	-13.1	665	-4.0	-2.8	-2.9	0.32	CTTS
OSHA 59	-27.0, -13.7	632	-4.1	-4.3	-3.5	0.38	CTTS
[K98c] Em* 53	-58.0	565	0.55	CTTS
BD +68 $^{\circ}$ 1118	-24.1	HAe
[K98c] Em* 58	-38.3	727	-3.5	-2.7	-2.1	...	CTTS
2MASS J 21225427	-7.3	385	0.80	CTTS
RNO 135	-5.0	310	-0.4	+0.9	+1.0	0.27	WTTS
NGC 7129 S V1	-19.4	620	CTTS
NGC 7129 S V2	-45.0	636	-2.6	-2.1	-3.7	...	CTTS
V391 Cep	-62.0	455	-29.8	-36.3	-31.4	...	CTTS
NGC 7129 S V3	-76.5	684	0.86	CTTS
[K98c] Em* 72	-34.0	687	-12.0	-11.1	-8.6	0.86	CTTS
HBC 731	-36.5	509	CTTS
V350 Cep	-70.0	495	-15.9	-19.7	-17.1	...	CTTS

Table 4—Continued

Id.	H α line		EW(CaII triplet)			EW(LiI) (\AA)	PMS Class
	EW (\AA)	$\Delta v(10\%)$ (km s^{-1})	8499 (\AA)	8545 (\AA)	8663 (\AA)		
GGD 33A	-93.8	764	-57.1	-64.9	-80.8	...	CTTS
[MMN2004b] 17	-11.0	515	0.37	CTTS
[K98c] Em* 73	-87.0	618	-0.8	-0.5		0.42	CTTS
BH Cep	-2.0	HAe
[K98c] Em* 95	-23.8	540	-2.0	-2.6	-1.9	0.42	CTTS
IRAS 22129+6949	-9.4, -9.1	446	0.25	CTTS
IRAS 22144+6923	-7.8	676	-2.5	0.9	0.9	0.22	CTTS
IRAS 22152+6947	2.4	0.20	WTTS?
BO Cep	-6.8	712	HAe
[K98c] Em* 109	-52.9	770	0.54	CTTS
[K98c] Em* 108	-17.4	520	0.50	CTTS
SV Cep	-8.0	0.27	HAe
IRAS F22219+7908	-31.0, 5.4	472	-1.9	-1.7	-1.3	...	HAe?
[K98c] Em* 119 N	-61.8	500	-19.2	-19.2	-13.6	0.44	CTTS
[K98c] Em* 119 S	-37.4	547	0.25	CTTS
[KP93] 2-1	-81.5	803	CTTS
[KP93] 2-39	-6.0	662	0.37	CTTS
[RD95] B	-27.4	461	-1.6	-1.2	-1.5	...	CTTS
[RD95] A	-24.6	537	-1.3	-1.1	-0.6	...	CTTS
[RD95] 2	-46.6	465	-3.8	-3.15	-2.42		CTTS
[RD95] 5	-19.8	324				0.58	CTTS
[KP93] 2-2	-69.5	538	-14.7	-15.3	-12.6	...	CTTS
IRAS 22355+7505	-30.8	620	CTTS
[KP93] 2-43	-3.2	316	WTTS
[KP93] 2-3	-23.6	746	0.36	CTTS
[ETM94] Star 3	-7.1	776	-2.0	-0.6	-0.9	0.26	CTTS
[KP93] 2-44	-12.7	479	0.44	CTTS
[KP93] 2-45	-33.2	432	0.32	CTTS
[KP93] 2-46	-57.8	566	0.55	CTTS
IRAS F22424+7450	-0.4	0.57	WTTS
[K98c] Em* 128	-83.5	630	-3.5	-3.5	-3.1	...	CTTS
IRAS 22480+7533	-25.7	673	-2.8	-3.2	-2.9	...	CTTS
[K98c] Em* 137	-44.3	484	CTTS
AS 507	-9.4	625	0.36	CTTS

Table 5. Photometric data of the observed stars. Numbers in parentheses indicate the mean absolute deviation of the derived magnitudes.

Id.	B	V	R _C	I _C	Comment
RNO 124	...	17.81 (0.25)	16.02 (0.12)	14.34 (0.12)	var. <i>BVR_CI_C</i>
PV Cep	19.27 (0.85)	17.46 (0.70)	15.98 (0.50)	14.60 (0.40)	var. <i>BVR_CI_C</i>
IRAS 20535+7439	13.44 (0.05)	12.37 (0.03)	11.76 (0.03)	11.11 (0.03)	
OSHA 42	18.36 (0.30)	16.74 (0.30)	15.38 (0.15)	14.06 (0.20)	var. <i>BVR_CI_C</i>
RNO 129 A	20.76 (0.05)	18.76 (0.03)	16.83 (0.04)	14.89 (0.02)	
RNO 129 SW	17.43 (0.07)	15.68 (0.07)	14.17 (0.07)	12.75 (0.07)	
RNO 129 NE	...	19.60 (...)	17.86 (...)	15.85 (...)	2.1'', 61°3
FT Cep	19.37 (1.10)	16.41 (0.83)	14.79 (0.80)	13.30 (0.95)	var. <i>BVR_CI_C</i>
FT Cep B	18.59 (0.07)	16.97 (0.01)	15.90 (0.01)	14.97 (0.02)	5.4'', 27°
[K98c] Em* 35	17.04 (0.07)	15.64 (0.11)	14.04 (0.25)	12.72 (0.25)	var. <i>VR_CI_C</i>
F21022+7729	20.30 (0.72)	19.89 (0.65)	18.09 (0.80)	16.22 (0.45)	var. <i>BVR_CI_C</i>
NGC 7023 RS 2	18.61 (0.05)	16.50 (0.03)	14.90 (0.03)	13.25 (0.07)	
NGC 7023 RS 2 B	20.37 (0.30)	18.26 (0.42)	16.63 (0.65)	14.98 (0.73)	var. <i>BVR_CI_C</i>
OSHA 48	15.64 (0.12)	14.31 (0.05)	12.75 (0.04)	11.51 (0.22)	var. <i>I_C</i>
OSHA 48 B	16.88 (0.26)	15.37 (0.30)	13.85 (0.15)	12.66 (0.12)	1.5'', 86°
OSHA 49	17.97 (0.06)	16.58 (0.05)	14.89 (0.05)	13.38 (0.08)	
OSHA 50	18.07 (0.05)	17.11 (0.05)	15.38 (0.05)	13.86 (0.05)	
OSHA 50 B	19.43 (...)	18.44 (...)	16.599 (0.11)	14.702 (0.14)	1.4'', 81°
LkHα 425	17.00 (0.05)	15.95 (0.02)	15.04 (0.02)	13.93 (0.02)	
SX Cep	16.21 (0.16)	14.67 (0.30)	13.53 (0.36)	12.40 (0.38)	var. <i>BVR_CI_C</i>
NGC 7023 RS 5	19.09 (0.10)	17.29 (0.10)	15.84 (0.51)	14.35 (0.60)	var. <i>BVR_CI_C</i>
NGC 7023 RS 5 B	19.08 (...)	17.501 (...)	1.5'', 158°
HZ Cep	17.00 (0.10)	15.22 (0.06)	14.01 (0.10)	12.76 (0.35)	var. <i>I_C</i>
FU Cep	17.70 (1.72)	16.13 (0.67)	14.83 (0.51)	13.47 (0.03)	var. <i>BVR_C</i>
PRN S3	21.86 (0.20)	18.94 (0.21)	16.73 (0.34)	15.11 (0.05)	var. <i>BVR_CI_C</i>
OSHA 53	15.88 (0.12)	14.37 (0.16)	13.35 (0.14)	12.47 (0.15)	var. <i>BVR_CI_C</i>
FV Cep	15.58 (0.55)	14.45 (0.40)	13.56 (0.29)	12.63 (0.43)	var. <i>BVR_CI_C</i>
LkHα 428 N	18.84 (0.30)	16.89 (0.06)	15.32 (0.01)	13.68 (0.01)	
LkHα 428 S	19.91 (0.30)	17.73 (0.02)	15.86 (0.01)	13.95 (0.05)	2.1'', 166°
FW Cep	16.17 (0.10)	14.83 (0.01)	13.83 (0.03)	12.98 (0.03)	
NGC 7023 RS 10	16.92 (0.07)	15.81 (0.05)	15.04 (0.05)	14.46 (0.06)	
[K98c] Em* 46	17.11 (0.05)	15.39 (0.04)	14.34 (0.02)	12.99 (0.02)	
[K98c] Em* 46B	17.50 (0.10)	15.22 (0.08)	1.0'', 270°
EH Cep	13.28 (0.07)	12.16 (0.02)	11.42 (0.02)	10.81 (0.02)	
OSHA 59	15.47 (0.07)	13.99 (0.05)	13.06 (0.02)	12.21 (0.02)	
[K98c] Em* 53	15.83 (0.10)	14.83 (0.12)	13.92 (0.12)	13.06 (0.14)	var. <i>BVR_CI_C</i>
BD +68°1118	10.08 (0.04)	9.94 (0.04)	9.811 (0.03)	9.750 (0.03)	
[K98c] Em* 58	18.79 (0.15)	17.62 (0.20)	16.77 (0.12)	16.03 (0.25)	var. <i>BVR_CI_C</i>
2MASS 21225427+6921345	...	19.27 (0.25)	17.78 (0.12)	16.23 (0.10)	
RNO 135	18.67 (0.03)	16.72 (0.01)	15.13 (0.01)	13.35 (0.01)	
NGC 7129 S V1	17.37 (0.35)	16.18 (0.36)	15.20 (0.40)	14.34 (0.50)	var. <i>BVR_CI_C</i>
NGC 7129 S V2	19.32 (0.50)	17.72 (0.45)	16.53 (0.42)	15.45 (0.36)	var. <i>BVR_CI_C</i>
V391 Cep	15.24 (0.06)	14.16 (0.04)	13.27 (0.04)	12.50 (0.03)	
NGC 7129 S V3	19.55 (0.45)	17.78 (0.42)	16.45 (0.50)	15.34 (0.55)	var. <i>BVR_CI_C</i>
NGC 7129 S V3 B	16.77 (...)	3.2'', 165°
[K98c] Em* 72	17.22 (0.06)	15.67 (0.03)	14.61 (0.04)	13.57 (0.03)	

Table 5—Continued

Id.	B	V	R _C	I _C	Comment
HBC 731	...	19.34 (0.15)	17.69 (0.12)	16.08 (0.23)	var. <i>BVR_CI_C</i>
V350 Cep	17.24 (0.10)	16.20 (0.10)	15.23 (0.06)	14.11 (0.07)	
GGD 33A	18.49 (...)	
[MMN2004b] 17	18.06 (0.10)	16.31 (0.04)	15.23 (0.36)	14.14 (0.01)	var. <i>R_C</i>
[K98c] Em* 73	15.58 (0.05)	14.59 (0.04)	13.66 (0.03)	12.90 (0.03)	
BH Cep	11.54 (0.05)	11.01 (0.03)	10.62 (0.03)	10.32 (0.03)	
[K98c] Em* 95	15.25 (0.10)	13.98 (0.15)	13.11 (0.12)	12.39 (0.07)	var. <i>VR_C</i>
[K98c] Em* 95 B	18.379 (...)	17.54 (...)	16.14 (...)	14.502 (...)	1.8'', 83°
IRAS 22129+6949	12.52 (0.01)	11.63 (0.04)	11.01 (0.02)	10.57 (0.02)	
IRAS 22144+6923	12.40 (0.04)	11.60 (0.02)	11.07 (0.02)	10.63 (0.02)	
IRAS 22152+6947 W	11.74 (0.03)	11.40 (0.02)	11.15 (0.03)	10.84 (0.03)	
BO Cep	11.98 (0.08)	11.55 (0.07)	11.16 (0.06)	10.84 (0.03)	
[K98c] Em* 109	16.30 (0.01)	14.96 (0.02)	13.94 (0.02)	13.18 (0.01)	
[K98c] Em* 108	14.47 (0.04)	13.27 (0.03)	12.43 (0.02)	11.87 (0.02)	
SV Cep	10.70 (0.10)	10.52 (0.12)	10.28 (0.06)	10.08 (0.05)	
IRAS 22219+7908	12.65 (0.06)	12.39 (0.04)	12.16 (0.02)	12.05 (0.02)	
[K98c] Em* 119 N	15.67 (0.08)	14.81 (0.08)	14.00 (0.06)	13.19 (0.07)	
[K98c] Em* 119 S	18.41 (0.07)	17.27 (0.07)	16.22 (0.11)	15.26 (0.01)	4'', 184°
[KP93] 2-1	17.12 (0.75)	15.42 (0.42)	13.80 (1.03)	12.53 (0.07)	var. <i>BVR_C</i>
[KP93] 39	17.34 (0.25)	15.89 (0.46)	14.38 (0.43)	13.31 (0.12)	var. <i>BVR_CI_C</i>
[RD95] B	...	22.99 (...)	20.22 (0.25)	17.76 (0.30)	var. <i>BVR_CI_C</i>
[RD95] A	...	20.94 (...)	19.12 (0.76)	16.09 (0.60)	var. <i>R_CI_C</i>
2MASS 22352542+7517562	18.93 (0.85)	17.20 (0.90)	15.59 (0.75)	14.15 (0.55)	var. <i>R_CI_C</i>
2MASS 22352722+7518019	19.40 (0.60)	17.66 (0.65)	15.83 (0.40)	14.45 (0.45)	var. <i>BVR_CI_C</i>
[KP93] 2-2	19.66 (1.60)	16.97 (1.85)	15.29 (0.45)	13.84 (1.10)	var. <i>BVR_CI_C</i>
IRAS 22355+7505	21.26 (0.60)	19.82 (0.45)	17.48 (0.34)	15.09 (0.50)	var. <i>BVR_CI_C</i>
[KP93] 2-43	19.18 (0.09)	16.87 (0.08)	15.17 (0.05)	13.57 (0.05)	
[KP93] 2-43B	19.37 (0.12)	18.71 (0.04)	16.71 (0.05)	14.86 (0.04)	5.2'', 245°5
[KP93] 2-3	16.50 (0.06)	15.04 (0.08)	14.01 (0.03)	13.13 (0.03)	
[ETM94] IRAS 22376+7455 Star 3	19.80 (0.25)	17.44 (0.06)	15.75 (0.06)	13.983 (0.05)	
[KP93] 2-44	17.65 (0.10)	16.10 (0.07)	14.90 (0.03)	13.62 (0.01)	
[KP93] 2-45	17.06 (0.12)	15.79 (0.02)	14.70 (0.34)	13.44 (0.45)	var. <i>R_CI_C</i>
[KP93] 2-46	19.05 (0.22)	17.01 (0.02)	15.24 (0.02)	13.56 (0.03)	
IRAS F22424+7450	14.37 (0.07)	13.22 (0.07)	12.48 (0.04)	11.86 (0.02)	
[K98c] Em* 128	16.87 (0.12)	15.66 (0.07)	14.70 (0.08)	13.69 (0.04)	
IRAS 22480+7533	12.95 (0.05)	12.00 (0.03)	11.41 (0.02)	10.87 (0.02)	
[K98c] Em* 137	17.66 (0.11)	16.48 (0.06)	15.321 (0.03)	13.76 (0.03)	
AS 507	11.17 (0.06)	10.22 (0.06)	9.63 (0.18)	9.16 (0.05)	
AS 507 B	16.93 (0.07)	16.08 (0.04)	14.69 (0.03)	12.71 (0.03)	9'', 156°

Table 6: Adopted cloud distances.

Cloud	D (pc)	References
L 1147 / L 1158	325	Straizys et al. (1992)
NGC 7023	282	Zdanavičius et al. (2009)
L 1228	200	Kun (1998)
L 1251	320	average from Kun (1998) and Balázs et al. (2004)
L 1219	400	Racine (1968)
L 1261 / L 1262	180	Kun (1998)
NGC 7129	800	Ábrahám et al. (2000)

Table 7. Parameters of the observed stars, derived from our optical data.

Star	A_V (mag)	$L_{\text{bol}}(L_{\odot})$	T_{eff} (K)	M_* (M_{\odot})	Age (Myr)	$\log \dot{M}_d$ ($M_{\odot} \text{ yr}^{-1}$)		
						$\Delta V(\text{H}\alpha)$	EW(H α)	EW(8542)
L1228								
F21022	5.90	0.34	3720	0.5	2.8	−4.98	−7.29	−7.21
OSHA 42	3.42	0.49	3850	0.6	2.8	−6.90	−6.97	−7.55
[K98c] Em* 35	0.92	0.34	3580	0.35	2.0	−8.36	−8.30	...
OSHA 48	2.89	2.83	4350	1.2	1.0	−8.60	−6.96	...
OSHA 49	2.26	0.38	3720	0.5	3.0	−9.11	−8.60	...
OSHA 50	3.05	0.28	3850	0.60	4.5	−7.82	−6.97	−6.87
[PRN2004] S3	4.04	0.21	3720	0.5	4.0	−7.94	−8.53	...
OSHA 53	1.55	0.57	4350	0.95	10.0	−7.56	−7.67	...
OSHA 59	1.74	0.67	4350	1.0	6.0	−6.49	−7.39	...
RNO 129 SW	4.20	0.42	3720	0.5	3.0	−6.58	−7.12	−6.69
RNO 129 NE	4.40	0.42	3580	0.35	3.0	−6.24	−7.41	−7.26
RNO 129 A	4.27	0.22	3650	0.42	1.2	−12.47	−11.95	...
[K98c] Em* 46	0.00	0.16	3580	0.35	2.5	−9.27	−9.39	...
NGC 7023								
FT Cep	5.85	6.33	5080	2.1	1.2	−7.03	−7.08	−6.90
FU Cep	1.82	0.48	3720	0.48	1.6	−5.94	−7.05	−7.21
LkH α 425	1.47	0.25	3850	0.6	5.0	−7.12	−7.46	−7.15
NGC 7023 RS2	3.65	1.82	3850	0.6	0.5	−7.31	−7.26	−8.21
NGC 7023 RS2B	4.41	0.60	3850	0.6	2.0	−7.81	−7.19	...
NGC 7023 RS5	2.83	0.41	3580	0.38	1.3	−7.30	−7.63	−7.69
HZ Cep	1.74	0.75	3850	0.6	1.5
SX Cep	1.46	0.89	4060	0.8	2.1
LkH α 428 N	4.47	2.02	4060	0.8	0.8	−6.56	−6.87	−7.02
LkH α 428 S	0.68	0.15	3305	0.2	1.5	−8.93	−8.92	...
FV Cep	1.27	0.63	4350	1.0	7.0	−8.78	−8.10	...
FW Cep	1.52	0.54	4350	1.0	8.5	−6.82	−8.68	...
NGC 7023 RS 10	0.00	0.07	4590	−9.66	−10.22	...
EH Cep	1.39	3.41	4900	1.8	2.9	−6.18	−6.76	−6.84
L1251								
[KP93] 2-1	4.67	6.61	4900	2.1	0.9	−4.88	−5.83	...
[KP93] 2-39	1.25	0.44	3850	0.6	3.0	−7.46	−8.63	...
[KP93] 2-2	2.01	0.43	3580	0.38	1.1	−7.35	−7.23	−6.78
[KP93] 3-10	6.16	1.28	3370	0.2	0.1	−5.48	−6.24	...
[RD95] A	8.88	2.24	4060	0.8	0.8	−7.36	−7.09	−7.22
[RD95] B	9.88	1.03	3850	0.6	0.9	−8.05	−7.11	−7.53
[RD95] 2	3.19	0.62	3525	0.35	0.8	−8.01	−6.15	−6.24
[RD95] 5	3.19	0.43	3580	0.6	3.0	−9.24	−7.11	...

Table 7—Continued

Star	A_V (mag)	$L_{\text{bol}}(L_{\odot})$	T_{eff} (K)	M_* (M_{\odot})	Age (Myr)	$\log \dot{M}_d$ ($M_{\odot} \text{ yr}^{-1}$)		
						$\Delta V(\text{H}\alpha)$	EW(H α)	EW(8542)
[KP93] 2-43	4.74	2.25	4350	1.2	1.0	−9.31	−9.31	...
[ETM94] Star 3	6.47	4.49	4900	2.0	1.8	−5.14	−7.47	...
[KP93] 2-3	1.21	0.50	4060	0.8	4.0	−5.42	−7.91	...
[KP93] 2-44	1.08	0.31	3650	0.41	2.5	−7.87	−8.76	...
[KP93] 2-45	1.62	0.49	3720	0.5	1.8	−8.31	−7.54	...
[KP93] 2-46	5.47	4.02	4350	1.2	0.5	−7.09	−6.24	...
IRAS 22424	0.44	1.00	4590	1.2	7.5	...	−9.29	...
IRAS 22480	0.79	3.00	5080	1.5	4.0	−6.51	−6.77	−6.99
[K98c] Em* 128	1.39	0.34	3850	0.6	4.0	−6.50	−7.73	−8.11
G 109+11 association								
BD+68° 1118	0.99	21.40	8970	2.0	7.0
[K98c] Em* 53	1.59	1.65	4350	1.2	1.5	−7.10	−7.37	−7.60
[K98c] Em* 58	1.34	0.10	4060	0.6	...	−5.60	−9.26	−9.21
2MASS 212254	5.66	0.87	4730	1.0	20:	−8.72	−8.88	...
[K98c] Em* 73	0.57	0.69	4060	0.8	3.0	−6.61	−7.20	−8.47
BH Cep	0.62	8.20	6440	1.5	6.0	...	−7.85	...
BO Cep	0.49	4.75	6440	1.35	15.0	...	−7.59	...
IRAS 22129	0.72	5.90	5250	1.8	3.0	−8.18	−7.01	...
IRAS 22144	0.21	4.88	6360	1.5	5.0	−6.08	−7.44	...
IRAS 22152	0.00	5.07	6440	1.3	10.0
[K98c] Em* 119N	0.90	0.69	4350	1.0	5.0	−7.70	−7.60	−7.20
[K98c] Em* 119S	2.89	0.33	5250	0.85	...	−7.27	−8.48	...
SV Cep group								
[K98c] Em* 95	0.40	2.22	4350	1.1	3.0	−7.33	−7.57	−7.53
[K98c] Em* 108	1.15	3.01	4900	2.0	1.5	−7.52	−7.22	...
[K98c] Em* 109	3.12	2.59	4900	1.5	3.5	−5.19	−6.66	...
SV Cep	1.48	44.67	8970	2.4	4.0	...	−6.63	...
NGC 7129								
V350 Cep	1.20	1.27	3850	0.58	0.5	−7.74	−6.99	−6.99
GGD 33a	2.84	0.06	3850	0.4	...	−5.52	−9.13	−8.29
[MMN2004b] 17	1.00	1.06	3720	0.45	0.5	−7.56	−8.41	...
HBC 731	7.71	6.53	4900	2.0	1.0	−7.62	−7.45	...
V391 Cep	0.96	4.76	4350	1.15	0.2	−8.10	−6.80	−6.25
NGC 7129 S V1	0.92	0.81	4060	0.8	2.5	−7.47	−8.55	...
NGC 7129 S V2	1.38	0.41	3850	0.6	3.0	−7.12	−8.63	−8.61
NGC 7129 S V3	3.50	1.40	4350	1.15	2.5	−6.69	−7.59	...
[K98c] Em* 72	3.05	5.70	4590	1.6	0.5	−5.97	−5.91	−5.96

Table 7—Continued

Star	A_V (mag)	$L_{\text{bol}}(L_{\odot})$	T_{eff} (K)	M_* (M_{\odot})	Age (Myr)	$\log \dot{M}_d$ ($M_{\odot} \text{ yr}^{-1}$)		
						$\Delta V(\text{H}\alpha)$	EW(H α)	EW(8542)
Small groups and dispersed stars								
RNO 124	6.53	0.92	5250	1.4	3.0	−6.64	−7.57	−7.43
PV Cep	4.87	0.90	5250	1.1	...	−7.87	−7.08	−6.40
IRAS F20535	1.76	4.04	6200	1.35	9.0	−8.60	−7.76	...
RNO 135	2.49	0.34	3470	0.30	1.0	−9.36	−8.58	...
IRAS F22219	1.17	5.33	9230	2.0	...	−7.94	−7.67	...
[K98c] Em* 137	2.59	0.20	3580	0.38	5.0	−7.84	−7.45	...
AS 507	1.07	5.77	5860	1.55	3.1	−6.55	−6.70	...

Column 1: Name of the star; Col. 2: The visual extinction A_V , derived from the color excesses; Col. 3: the bolometric luminosity of the star, derived from the optical data; Col. 3: T_{eff} derived from the spectral classification; Col. 4: Mass of the star derived from the HRD; Col. 5: Age of the star, derived from the HRD; Cols. 6–9: Logarithm of accretion rates from the disk in $M_{\odot} \text{ yr}^{-1}$, derived from the 10% width of the H α line (Natta et al. 2004), from the luminosity of H α emission line, and the CaII λ 8542 line (Dahm 2008), respectively.

Table 8. Median properties of observed stars for individual regions

Region	A_V (mag)	T_{eff} (K)	M_* (M_\odot)	Age (Myr)	$\log(\dot{M}_{\text{acc}}^d)$ ($M_\odot \text{ yr}^{-1}$)	α_{24-K}	λ_{turnoff} μm	N
NGC 7023	1.6	3850	0.6	1.6	−7.3	0.98	3.6	14
L 1228	3.1	3720	0.5	3.0	...	0.90	3.6	13
L 1228 S	2.3	3720	0.5	3.0	−8.3	0.90	5.8	7
L 1251	3.2	3850	0.6	1.8	−7.1	0.93	2.2	17
L 1251 C	4.7	3850	0.6	0.9	−7.1	0.93	1.2	8
L 1251 E	1.6	4060	0.8	1.8	−7.5	0.94	5.8	5
G 109+11 ass.	1.0	5250	1.5	6.0	...	0.28	...	12
SV Cep group	1.3	4900	1.7	3.0	...	0.68	...	4
NGC 7129	1.4	4060	0.8	1.0	−7.5	0.29	1.6	9

The quantities listed in Cols. 2–6 are determined from the present spectroscopic and photometric observations; Columns 7 and 8 show the median SED slope α_{24-K} , and λ_{turnoff} , respectively. Column 9 shows the number of group members studied.